

UNSCENTED KALMAN INVERSION: EFFICIENT GAUSSIAN APPROXIMATION TO THE POSTERIOR DISTRIBUTION

DANIEL Z. HUANG* AND JIAOYANG HUANG†

Abstract. The unscented Kalman inversion (UKI) method presented in [1] is a general derivative-free approach for the inverse problem. UKI is particularly suitable for inverse problems where the forward model is given as a black box and may not be differentiable. The regularization strategies, convergence property, and speed-up strategies [1, 2] of the UKI are thoroughly studied, and the method is capable of handling noisy observation data and solving chaotic inverse problems. In this paper, we study the uncertainty quantification capability of the UKI. We propose a modified UKI, which allows to well approximate the mean and covariance of the posterior distribution with an uninformative prior for identifiable (well-posed) inverse problems. Theoretical guarantees for both linear and nonlinear inverse problems are presented. Numerical results, including learning of permeability parameters in subsurface flow and of the Navier-Stokes initial condition from solution data at positive times are presented. The results obtained by the UKI require only $\mathcal{O}(10)$ iterations, and match well with the expected results obtained by the Markov Chain Monte Carlo method.

Key words. Inverse Problem, Uncertainty Quantification, Kalman Filter, Bayesian Inference, Unscented Kalman Inversion

AMS subject classifications. 60G35, 62F15, 62M20, 65N21

1. Introduction. Inverse problems are ubiquitous in engineering and science applications. These include, to name only a few, global climate model calibration [3, 4, 5], material constitutive relation calibration [6, 7, 8], seismic inversion in geophysics [9, 10], and medical tomography [11, 12]. These problems may feature multiple scales and may include chaotic and turbulent phenomena, and hence the forward models are very expensive to evaluate. Moreover, the observation data are noisy and uncertainty quantification is important.

Inverse problems can be formulated as recovering unknown parameters $\theta \in \mathbb{R}^{N_\theta}$ from the noisy observation $y \in \mathbb{R}^{N_y}$, as following

$$(1.1) \quad y = \mathcal{G}(\theta) + \eta,$$

where \mathcal{G} denotes a forward operator mapping parameters to observations, and η denotes the observational error, which might depend on θ or y . An estimated distribution of $\eta \sim \mathcal{N}(0, \Sigma_\eta)$ is given.

From optimization viewpoint, the inverse problem can be formulated to the following nonlinear least-square optimization problem [13]:

$$(1.2a) \quad \Phi_R(\theta, y) := \Phi(\theta, y) + \frac{1}{2} \|\Sigma_0^{-\frac{1}{2}}(\theta - r_0)\|^2,$$

$$(1.2b) \quad \Phi(\theta, y) := \frac{1}{2} \|\Sigma_\eta^{-\frac{1}{2}}(y - \mathcal{G}(\theta))\|^2,$$

where Φ_R and Φ are regularized and non-regularized objective functions, respectively. $\Sigma_\eta \succ 0$ is strictly positive-definite and normalizes the model-data misfit. r_0 and $\Sigma_0 \succ 0$ encode prior mean and covariance information about θ . From Bayesian viewpoint, θ and y are treated as random variables, and the inverse problem can be formulated as posterior distribution approximation problem [14, 15]:

$$(1.3) \quad \mu(d\theta) = \frac{1}{Z(y)} e^{-\Phi(\theta, y)} \mu_0(d\theta),$$

where $\mu_0(d\theta)$ is the prior and $Z(y)$ is the normalization constant:

$$(1.4) \quad Z(y) = \int e^{-\Phi(\theta, y)} \mu_0(d\theta).$$

The optimization viewpoint and the Bayesian viewpoint are linked via the fact that the minimizer of the nonlinear least-square optimization problem $\Phi(\theta, y)$ coincides with the maximum a posteriori (MAP) estimator of (1.3) with an uninformative prior, and the minimizer of the regularized nonlinear least-square optimization problem $\Phi_R(\theta, y)$ coincides with the MAP estimator of (1.3).

*California Institute of Technology, Pasadena, CA (dzhuang@caltech.edu).

†New York University, New York, NY (jh4427@nyu.edu).

Kalman inversion methods, which take advantage of Kalman filtering [16, 17, 18, 19, 20], a powerful state estimation technique, are able to unify both optimization and Bayesian viewpoints. This methodology, including but not limited to unscented (UKI) and ensemble (EKI) Kalman inversions, used as a non-intrusive optimization method for parameter estimation, originates in the papers [21, 22, 23, 24, 25, 26]. For inverse problems in general, they are attractive because they are derivative-free, and hence introduce a significant flexibility in the forward solver design. Therefore, Kalman inversions are suitable for complex multiphysics problems requiring coupling of different solvers [27, 28, 29, 30, 31] and methods containing discontinuities (i.e., immersed/embedded boundary method [32, 33, 34, 35] and adaptive mesh refinement [36, 37]). However, as for Bayesian inference, due to the Gaussian ansatz in Kalman filtering, the capability of Kalman inversions to quantify uncertainties or approximate posterior distribution remains unclarified. This work focuses on understanding and improving the capability of Kalman inversions, specifically the UKI, to provide accurate Gaussian approximations to the posterior distribution.

1.1. Literature Review. The Kalman filter [16] and its variants, including but not limit to extended Kalman filter [17], ensemble Kalman filter [18], unscented Kalman filter [19, 23], and cubature Kalman filter [20] are developed to sequentially update the probability distribution of states in partially observed dynamics. Kalman filtering is a two-step procedure: the prediction step, where the state is computed forward in time; the analysis step, where the state and its uncertainty are corrected to take into account the observation. In the analysis step, Kalman filters use Gaussian ansatz to formulate Kalman gain to assimilate the observation and update the distribution, which is valid only for linear state estimation problems, where the probability distribution of states remains Gaussian given Gaussian priors. Therefore, Kalman filters do not produce correct estimate of posterior distribution for non-Gaussian problems [38]. However, numerous applications of Kalman filters, including weather forecasts [18, 39, 40] and guidance, navigation, and control of vehicles [17, 19, 20] demonstrate empirically that Kalman filters can not only calibrate the model prediction, but also provides uncertainty information for nonlinear state estimation problems, specifically the mean and covariance estimation. To get better posterior estimation, particle filters [41] are needed, where the distribution is represented by a large number of random samples. Most of particle filters consist of prediction step and analysis step. In the analysis step, these samples and their associated weights are corrected with the information provided by the observation. The standard particle filter corrects the weights of each sample following Bayes' theorem. Different correction methods are proposed, which lead to the random maximum likelihood method [42, 43], the nonparametric ensemble transform method [44], and etc.

Filter methods can also be used to estimate the parameters, where the filters are recursively applied to an artificial stochastic dynamical system generally with identity state transition matrix. This leads to different inversion methods, to name only a few, sequential Monte Carlo sampler (SMC) [45, 46, 47], random maximum likelihood method [43, 24], ensemble Kalman inversion [48, 49, 25], unscented Kalman inversion [23, 1, 2]. Besides estimating the parameters by minimizing the nonlinear least square problems (1.2), these inversion methods are derived in the Bayesian framework, and therefore, have the potential to deliver sensitivity and uncertainty information.

This paper mainly focuses on Kalman inversion methodology, which is a general derivative-free approach to solving the inverse problem. So far, the Kalman inversions have mainly been used for parameter estimation [25, 50, 51, 52, 53, 54] rather than for Bayesian inference for quantifying uncertainty. Due to the Gaussian ansatz and the iterative nature, Kalman inversions generally do not converge to the posterior distribution. Specifically, the mean converges but not the covariance in the nonlinear case. Negative numerical evidences are reported in [55, 56]. In the present work, we improve the UKI by modifying the stochastic dynamical system through iteratively updating the artificial evolution error covariance matrix. And we demonstrate both theoretically and numerically that equipping with the modified stochastic dynamical system, the Kalman inversion, specifically the UKI, is able to provide good Gaussian approximations to the posterior distribution with an uninformative prior for both linear and nonlinear inverse problems under certain regularity assumptions.

1.2. Our Contributions. Our main contribution is the development of theoretical and numerical understanding about UKI for Bayesian inference for quantifying uncertainty.

- We modify the stochastic dynamical system of Kalman inversions proposed in [1, 2] by iteratively updating the artificial evolution covariance matrix, which enables better approximating the posterior covariance matrix.

- With this modification, for linear inverse problems, we prove the exponential convergence of the UKI. The mean converges to a minimizer of Φ and the precision matrix converges to the posterior precision matrix with an uninformative prior.
- With this modification, for nonlinear inverse problems, we prove the UKI approximates well with the mean and covariance of the posterior distribution with an uninformative prior, when the forward operator \mathcal{G} is bijective and satisfies certain regularity conditions.
- We demonstrate on model problems with 1 to 32 parameters that the UKI delivers similar mean and covariance comparing to Markov Chain Monte Carlo method. We believe the UKI can be used for large-scale Bayesian inference, which is demonstrated on a Navier-Stokes initial condition recovery problem with 100 parameters.
- For the UKI, all tests converge within $\mathcal{O}(10)$ iterations with no empirical variance inflation or early stopping needed.

The remainder of the paper is organized as follows. In [section 2](#), an overview of Kalman inversion algorithm and the modified UKI are presented. In [section 3](#), theoretical results for the modified UKI are presented. Numerical applications are provided in [section 4](#), that empirically confirm the theories and demonstrate the effectiveness of the UKI for Bayesian inference for quantifying uncertainty.

2. The Algorithm. Kalman inversion methods pair the parameter-to-data map \mathcal{G} with a stochastic dynamical system for the parameter and then employ techniques from filtering to estimate the parameter given the data. Consider the following stochastic dynamical system,¹

$$(2.1a) \quad \text{evolution:} \quad \theta_{n+1} = \theta_n + \omega_{n+1}, \quad \omega_{n+1} \sim \mathcal{N}(0, \Sigma_\omega)$$

$$(2.1b) \quad \text{observation:} \quad y_{n+1} = \mathcal{G}(\theta_{n+1}) + \nu_{n+1}, \quad \nu_{n+1} \sim \mathcal{N}(0, \Sigma_\nu)$$

where θ_{n+1} is the unknown state vector, and y_{n+1} the observation, the artificial evolution error ω_{n+1} and artificial observation error ν_{n+1} are mutually independent, zero-mean Gaussian sequences with covariances Σ_ω and Σ_ν , respectively. Let denote $Y_{n+1} := \{y_1, y_2, \dots, y_{n+1}\}$, the observation set at time $n+1$. Filtering techniques are employed to approximate μ_{n+1} , the conditional distribution of $\theta_{n+1}|Y_{n+1}$. And the updating of $\{\mu_n\}$ is through the prediction and analysis steps [[57](#), [58](#)]: $\mu_n \mapsto \hat{\mu}_{n+1}$, and then $\hat{\mu}_{n+1} \mapsto \mu_{n+1}$, where $\hat{\mu}_{n+1}$ is the distribution of $\theta_{n+1}|Y_n$.

2.1. Gaussian Approximation. This conceptual algorithm maps Gaussians into Gaussians. In the prediction step, assume that $\mu_n \approx \mathcal{N}(m_n, C_n)$, then under (2.1a), $\hat{\mu}_{n+1} = \mathcal{N}(\hat{m}_{n+1}, \hat{C}_{n+1})$ is also Gaussian and satisfies

$$(2.2) \quad \hat{m}_{n+1} = \mathbb{E}[\theta_{n+1}|Y_n] = m_n \quad \hat{C}_{n+1} = \text{Cov}[\theta_{n+1}|Y_n] = C_n + \Sigma_\omega.$$

In the analysis step, we assume that the joint distribution of $\{\theta_{n+1}, y_{n+1}\}|Y_n$ can be approximated by a Gaussian distribution

$$(2.3) \quad \mathcal{N}\left(\begin{bmatrix} \hat{m}_{n+1} \\ \hat{y}_{n+1} \end{bmatrix}, \begin{bmatrix} \hat{C}_{n+1} & \hat{C}_{n+1}^{\theta p} \\ \hat{C}_{n+1}^{\theta p T} & \hat{C}_{n+1}^{pp} \end{bmatrix}\right),$$

where

$$(2.4) \quad \begin{aligned} \hat{y}_{n+1} &= \mathbb{E}[y_{n+1}|Y_n] = \mathbb{E}[\mathcal{G}(\theta_{n+1})|Y_n], \\ \hat{C}_{n+1}^{\theta p} &= \text{Cov}[\theta_{n+1}, y_{n+1}|Y_n] = \text{Cov}[\theta_{n+1}, \mathcal{G}(\theta_{n+1})|Y_n], \\ \hat{C}_{n+1}^{pp} &= \text{Cov}[y_{n+1}|Y_n] = \text{Cov}[\mathcal{G}(\theta_{n+1})|Y_n] + \Sigma_\nu. \end{aligned}$$

Conditioning the Gaussian in (2.3) to find $\theta_{n+1}|Y_n, y_{n+1} = \theta_{n+1}|Y_{n+1}$, gives the following expressions for the mean m_{n+1} and covariance C_{n+1} of the approximation to μ_{n+1} :

$$(2.5) \quad \begin{aligned} m_{n+1} &= \hat{m}_{n+1} + \hat{C}_{n+1}^{\theta p} (\hat{C}_{n+1}^{pp})^{-1} (y_{n+1} - \hat{y}_{n+1}), \\ C_{n+1} &= \hat{C}_{n+1} - \hat{C}_{n+1}^{\theta p} (\hat{C}_{n+1}^{pp})^{-1} \hat{C}_{n+1}^{\theta p T}. \end{aligned}$$

¹In the present study, we focus on the dynamics without regularization, which is equivalent to setting $\alpha = 1$ in [[1](#), [2](#)].

Remark 2.1. Assume $\mu_n = \mathcal{N}(m_n, C_n)$, for linear \mathcal{G} , the Gaussian approximation $\mathcal{N}(m_{n+1}, C_{n+1})$ in (2.5) is exact, namely $\mu_{n+1} = \mathcal{N}(m_{n+1}, C_{n+1})$; for nonlinear but close to linear \mathcal{G} , the Gaussian approximation $\mathcal{N}(m_{n+1}, C_{n+1})$ is a good approximation of the conditional distribution μ_{n+1} , an upper bound of the Kullback–Leibler divergence between them is presented in [Appendix A](#).

As a method for solving the inverse problem (1.1), it is implemented by assuming all observations $\{y_n\}$ are identical to y ($Y_n = y$) and iterating in n . Equations (2.2)–(2.5) establish a conceptual algorithm for application of Gaussian approximation to solve the inverse problems. And the integrals appearing in (2.4) are approximated by the extended or unscented approach, which is detailed in the following subsections.

2.2. Extended Kalman Inversion (ExKI). ExKI approximates integrals in (2.4) analytically by applying first-order Taylor expansion to $\mathcal{G}(\theta_{n+1})$ at the conditional expectation $\mathbb{E}[\theta_{n+1}|y] = \hat{m}_{n+1}$,

$$(2.6) \quad \mathcal{G}(\theta_{n+1}) \approx \mathcal{G}(\hat{m}_{n+1}) + d\mathcal{G}(\hat{m}_{n+1})(\theta_{n+1} - \hat{m}_{n+1}).$$

And the iteration procedure of ExKI becomes:

- Prediction step :

$$(2.7) \quad \hat{m}_{n+1} = m_n \quad \hat{C}_{n+1} = C_n + \Sigma_\omega.$$

- Analysis step :

$$(2.8) \quad \begin{aligned} \hat{y}_{n+1} &= \mathcal{G}(\hat{m}_{n+1}), \\ \hat{C}_{n+1}^{\theta p} &= \hat{C}_{n+1} d\mathcal{G}(\hat{m}_{n+1})^T, \\ \hat{C}_{n+1}^{pp} &= d\mathcal{G}(\hat{m}_{n+1}) \hat{C}_{n+1} d\mathcal{G}(\hat{m}_{n+1})^T + \Sigma_\nu, \\ m_{n+1} &= \hat{m}_{n+1} + \hat{C}_{n+1}^{\theta p} (\hat{C}_{n+1}^{pp})^{-1} (y - \hat{y}_{n+1}), \\ C_{n+1} &= \hat{C}_{n+1} - \hat{C}_{n+1}^{\theta p} (\hat{C}_{n+1}^{pp})^{-1} \hat{C}_{n+1}^{\theta p T}. \end{aligned}$$

2.3. Unscented Kalman Inversion (UKI). UKI approximates the integrals in (2.4) by means of deterministic quadrature rules. This is the idea of the unscented transform [[19](#), [23](#)] which we now define.

DEFINITION 2.2 (Modified Unscented Transform [[1](#)]). *Let denote Gaussian random variable $\theta \sim \mathcal{N}(m, C) \in \mathbb{R}^{N_\theta}$, $2N_\theta + 1$ symmetric sigma points are chosen deterministically:*

$$(2.9) \quad \theta^0 = m \quad \theta^j = m + c_j [\sqrt{C}]_j \quad \theta^{j+N_\theta} = m - c_j [\sqrt{C}]_j \quad (1 \leq j \leq N_\theta),$$

where $[\sqrt{C}]_j$ is the j th column of the Cholesky factor of C . The quadrature rule approximates the mean and covariance of the transformed variable $\mathcal{G}_i(\theta)$ as follows,

$$(2.10) \quad \mathbb{E}[\mathcal{G}_i(\theta)] \approx \mathcal{G}_i(\theta^0) \quad Cov[\mathcal{G}_1(\theta), \mathcal{G}_2(\theta)] \approx \sum_{j=1}^{2N_\theta} W_j^c (\mathcal{G}_1(\theta^j) - \mathbb{E}\mathcal{G}_1(\theta)) (\mathcal{G}_2(\theta^j) - \mathbb{E}\mathcal{G}_2(\theta))^T.$$

Here these constant weights are

$$(2.11) \quad \begin{aligned} c_1 = c_2 \cdots = c_{N_\theta} &= \sqrt{N_\theta + \lambda} \quad W_j^c = \frac{1}{2(N_\theta + \lambda)} \quad (j = 1, \dots, 2N_\theta) \\ \lambda &= a^2(N_\theta + \kappa) - N_\theta \quad \kappa = 0 \quad a = \min\left\{\sqrt{\frac{4}{N_\theta + \kappa}}, 1\right\}. \end{aligned}$$

Consider the Gaussian approximation algorithm defined by (2.2)–(2.5). By utilizing the aforementioned quadrature rule, the iteration procedure of the UKI becomes:

- Prediction step :

$$\hat{m}_{n+1} = m_n \quad \hat{C}_{n+1} = C_n + \Sigma_\omega.$$

- Generate sigma points :

$$\begin{aligned}\hat{\theta}_{n+1}^0 &= \hat{m}_{n+1}, \\ \hat{\theta}_{n+1}^j &= \hat{m}_{n+1} + c_j [\sqrt{\hat{C}_{n+1}}]_j \quad (1 \leq j \leq N_\theta), \\ \hat{\theta}_{n+1}^{j+N_\theta} &= \hat{m}_{n+1} - c_j [\sqrt{\hat{C}_{n+1}}]_j \quad (1 \leq j \leq N_\theta).\end{aligned}$$

- Analysis step :

$$(2.12) \quad \begin{aligned}\hat{y}_{n+1}^j &= \mathcal{G}(\hat{\theta}_{n+1}^j) \quad \hat{y}_{n+1} = \hat{y}_{n+1}^0, \\ \hat{C}_{n+1}^{\theta p} &= \sum_{j=1}^{2N_\theta} W_j^c (\hat{\theta}_{n+1}^j - \hat{m}_{n+1})(\hat{y}_{n+1}^j - \hat{y}_{n+1})^T, \\ \hat{C}_{n+1}^{pp} &= \sum_{j=1}^{2N_\theta} W_j^c (\hat{y}_{n+1}^j - \hat{y}_{n+1})(\hat{y}_{n+1}^j - \hat{y}_{n+1})^T + \Sigma_\nu, \\ m_{n+1} &= \hat{m}_{n+1} + \hat{C}_{n+1}^{\theta p} (\hat{C}_{n+1}^{pp})^{-1} (y - \hat{y}_{n+1}), \\ C_{n+1} &= \hat{C}_{n+1} - \hat{C}_{n+1}^{\theta p} (\hat{C}_{n+1}^{pp})^{-1} \hat{C}_{n+1}^{\theta p T}.\end{aligned}$$

2.4. Choice of Hyperparameters. The hyperparameters r , Σ_ω and Σ_ν in the stochastic dynamical system (2.1) are chosen at the n -th iteration, as following

$$(2.13) \quad r = r_0 \quad \Sigma_\nu = 2\Sigma_\eta \quad \text{and} \quad \Sigma_\omega = C_n,$$

here r_0 is the prior mean. It is worth mentioning the artificial evolution error covariance Σ_ω is updated as the estimated covariance C_n . This choice of Σ_ω marks the key difference to the previous UKI discussed in [1, 2].

3. Theoretical Insights. The aforementioned Kalman inversion methodology recursively applies Gaussian approximation in each iteration to solve the inverse problem. A useful way to think of the iterative approach is through the following updating relation

$$\mu_{n+1}(d\theta) = \frac{1}{Z_n} \exp(-\Phi(\theta, y)) \mu_n(d\theta).$$

In the limit of large n , μ_n will tend to concentrate on minimizers of Φ ; this follows from the identity

$$\mu_n(d\theta) = \frac{1}{(\prod_{\ell=0}^{n-1} Z_\ell)} \exp(-n\Phi(\theta, y)) \mu_0(d\theta).$$

The prior information fades away, and therefore, Kalman inversion methodology generally does not converge to the posterior distribution $\theta|y$.

However, in this section, we will show that Kalman inversion with the hyperparameters defined in (2.13) provides an accurate Gaussian approximation to the posterior distribution $\theta|y$ with an **uninformative prior** under certain conditions.

3.1. The Linear Setting. In this subsection, we study the UKI in the context of linear inverse problems, for which $\mathcal{G}(\cdot) = G$. Thanks to the linearity, equations (2.4) are reduced to

$$\hat{y}_{n+1} = Gm_n, \quad \hat{C}_{n+1}^{\theta p} = \hat{C}_{n+1} G^T, \quad \text{and} \quad \hat{C}_{n+1}^{pp} = G\hat{C}_{n+1} G^T + \Sigma_\nu.$$

The update equations (2.5) become

$$(3.1) \quad \begin{aligned}m_{n+1} &= m_n + \hat{C}_{n+1} G^T (G\hat{C}_{n+1} G^T + \Sigma_\nu)^{-1} (y - Gm_n), \\ C_{n+1} &= \hat{C}_{n+1} - \hat{C}_{n+1} G^T (G\hat{C}_{n+1} G^T + \Sigma_\nu)^{-1} G\hat{C}_{n+1},\end{aligned}$$

with $\hat{C}_{n+1} = C_n + \Sigma_\omega$. We have the following theorem about the convergence of the Kalman inversion:

THEOREM 3.1. *Assume the prior covariance matrix $C_0 \succ 0$ is strictly positive definite. The iteration for the conditional mean m_n and precision matrix C_n^{-1} characterizing the distribution of $\theta_n|Y_n$ converges exponentially fast to limit m_∞, C_∞^{-1} . Furthermore the limiting mean m_∞ is a minimizer of the unregularized least squares functional Φ (1.2b); the limiting precision matrix $C_\infty^{-1} = G^T \Sigma_\eta^{-1} G$, which is the posterior precision matrix with an uninformative prior.*

Proof. The proof is in [Appendix B](#). □

Remark 3.2. When G has empty null space, which corresponds to an identifiable inverse problem, the posterior distribution with an uninformative prior exists. The covariance matrix $\{C_n\}$ converges to $(G^T \Sigma_\eta^{-1} G)^{-1}$, which is the posterior covariance matrix with the uninformative prior.

Remark 3.3. When G has non-empty null space, namely $G^T \Sigma_\eta^{-1} G$ is singular, and hence the posterior distribution with an uninformative prior does not exist. C_∞^{-1} is singular and therefore, the covariance matrix $\{C_n\}$ diverges to ∞ . We have the following bound

$$C_n \preceq 2^n C_0.$$

3.2. The Nonlinear Setting. In this subsection, we study the UKI in the context of nonlinear identifiable (well-posed) inverse problems. The following pull-back distribution bridges the posterior distribution (1.3) and the stationary Gaussian distribution obtained by the Kalman inversion.

DEFINITION 3.4 (Pull-back random variable). *Assume $N_\theta = N_y$, given a bijective function $\mathcal{G} : R^{N_\theta} \mapsto R^{N_y}$ and an arbitrary vector $y \in R^{N_y}$. For any random vector $\xi \in R^{N_y}$, the corresponding pull-back random variable is defined as*

$$(3.2) \quad \theta^\xi = \mathcal{G}^{-1}(y - \xi).$$

We have the following theorem about the posterior distribution $\theta|y$ with an uninformative prior defined in (1.3) and the pull-back distribution of $\theta^\eta = \mathcal{G}^{-1}(y - \eta)$:

THEOREM 3.5. *Consider the posterior density function $p(\theta|y)$ with an uninformative prior*

$$(3.3) \quad p(\theta|y) \sim \frac{1}{Z} e^{-\Phi(\theta, y)},$$

and the pull-back density function $p(\theta^\eta)$. We assume

1. the map \mathcal{G} is a bijection, hence, $N_\theta = N_y$ and \mathcal{G}^{-1} exists,
2. $\left| \det \frac{d\mathcal{G}^{-1}(\theta)}{d\theta} \right|$ has Lipschitz property:

$$(3.4) \quad \left| \left| \det \frac{d\mathcal{G}^{-1}(\theta_1)}{d\theta} \right| - \left| \det \frac{d\mathcal{G}^{-1}(\theta_2)}{d\theta} \right| \right| \leq c_0 \|\theta_1 - \theta_2\|^{c_1},$$

3. $\mathcal{G}^{-1}(\theta)$ does not grow too fast, and we have

$$\frac{1}{\sqrt{(2\pi)^{N_y} \det \Sigma_\eta}} \int e^{-\frac{1}{2}(y-\theta)^T \Sigma_\eta^{-1} (y-\theta)} \|\mathcal{G}^{-1}(\theta)\|^4 d\theta \leq c_2,$$

4. The normalization constant

$$Z = \int e^{-\Phi(\theta, y)} d\theta = \int e^{-\frac{1}{2}(y-\theta')^T \Sigma_\eta^{-1} (y-\theta')} \left| \det \frac{d\mathcal{G}^{-1}(\theta')}{d\theta} \right| d\theta' \text{ where } \theta' = \mathcal{G}(\theta)$$

exists and has positive lower bound $Z \geq c_3 > 0$,

5. c_i and N_θ are $\mathcal{O}(1)$ constants, and the spectral radius of Σ_η , $\rho(\Sigma_\eta)$ is small enough.

Then $p(\theta|y)$ and $p(\theta^\eta)$ have close mean and covariance, which satisfy

$$(3.5) \quad \|m - m^\eta\|_\infty = \mathcal{O}(\rho(\Sigma_\eta)^{c_1} \sqrt{\det \Sigma_\eta}) \quad \text{and} \quad \|C - C^\eta\|_\infty = \mathcal{O}(\rho(\Sigma_\eta)^{c_1} \sqrt{\det \Sigma_\eta}),$$

here m and C and m^η and C^η are the mean and covariance of $p(\theta|y)$ and $p(\theta^\eta)$, respectively.

Proof. The proof is in [Appendix C](#). □

We have the following theorem about the pull back distribution of θ^n and the ExKI,

THEOREM 3.6. *Assume $N_\theta = N_y$ and \mathcal{G} is a bijection. Any stationary mean and covariance m_*, C_* obtained by the ExKI, which satisfy that both $d\mathcal{G}(m_*)$ and C_* are non-singular, then*

$$(3.6) \quad m_* = \mathcal{G}^{-1}(y) \quad \text{and} \quad C_*^{-1} = d\mathcal{G}(m_*)^T \Sigma_\eta^{-1} d\mathcal{G}(m_*).$$

And they are the mean and covariance estimation of the pull-back random variable θ^n obtained by the extended Kalman filter.

Proof. The proof is in [Appendix D](#). □

Combining [Theorems 3.5](#) and [3.6](#), we have, in the presence of small observation error, the ExKI is able to well approximate the mean and covariance of the posterior distribution with an uninformative prior under certain conditions on the operator \mathcal{G} . The UKI [1] further applies averaging on the inverse function \mathcal{G} and its gradient $d\mathcal{G}$, which leads to $\mathcal{F}_u\mathcal{G}$ and $\mathcal{F}_u d\mathcal{G}$. By the analogy to the ExKI, the UKI is also able to approximate the mean and covariance of the posterior distribution with an uninformative prior under similar conditions.

Remark 3.7. Numerical studies presented in [subsections 4.3](#) and [4.4](#) indicate the UKI delivers good Gaussian approximation to the posterior distribution also for over-determined inverse problems.

Remark 3.8. Numerical studies presented in [subsection 4.1](#) indicate the injection and the Lipschitz continuity of \mathcal{G} are necessary for accurate posterior mean and covariance approximation.

4. Applications. In this section, we present numerical study of the UKI equipping with the stochastic dynamics [\(2.13\)](#) for approximating the posterior distribution. To be concrete, we initialize UKI with $\theta_0 \sim \mathcal{N}(m_0, C_0)$, where $m_0 = r_0$. It is worth mentioning r_0 is the prior mean but C_0 is generally not the prior covariance. Specific choices of r_0 and C_0 will differ between examples and will be spelled out in each example. For comparison, we also apply the Markov Chain Monte Carlo method (MCMC), specifically the random walk Metropolis algorithm, and the Sequential Monte Carlo method [[45](#), [46](#), [47](#)] (SMC).

- Nonlinear 1-parameter model problems: the behavior of the UKI is studied on different forward maps, including discontinuous functions, non-injective functions, and etc.
- Nonlinear 2-parameter model problem: this is counterexample against the ensemble Kalman filter [[55](#), [56](#)]. This problem demonstrates the effectiveness of the modified stochastic dynamical system, which enables the UKI to obtain accurate posterior approximation.
- Nonlinear high dimensional model problem: this is a well-studied Darcy flow inverse problem. The comparison between UKI and MCMC is presented, good agreement in terms of mean and covariance estimations is achieved.
- Navier-Stokes problem: this is a model data assimilation problem in oceanography and meteorology, where the initial condition is recovered from noisy observations of the vorticity field at later times.

The code is accessible online:

<https://github.com/Zhengyu-Huang/InverseProblems.jl>

4.1. Nonlinear 1-Parameter Model Problem. The performance of the UKI is studied numerically on the following nonlinear 1-parameter problems:

- Exponential problem:

$$y = \mathcal{G}(\theta) + \eta \quad \mathcal{G}(\theta) = \exp\left(\frac{\theta}{10}\right).$$

- Quadratic multimodal problem:

$$y = \mathcal{G}(\theta) + \eta \quad \mathcal{G}(\theta) = \theta^2.$$

- Cubic problem:

$$y = \mathcal{G}(\theta) + \eta \quad \mathcal{G}(\theta) = \theta^3.$$

- Sign discontinuous problem:

$$y = \mathcal{G}(\theta) + \eta \quad \mathcal{G}(\theta) = \text{sign}(\theta) + \theta^3.$$

- Hyperbola discontinuous problem:

$$y = \mathcal{G}(\theta) + \eta \quad \mathcal{G}(\theta) = \frac{1}{\theta}.$$

We assume the observation is generated as $y = \mathcal{G}(\theta_{ref})$, where the reference solution $\theta_{ref} = 2$. And the observation error is $\eta \sim \mathcal{N}(0, 0.1^2)$. For Bayesian inverse problems, we assume the prior distribution is $\mathcal{N}(-1, 10^2)$, where the prior mean -1 is on a different branch for these discontinuous problems. It is worth noticing, for these inverse problems, the observation error is small, and the prior is almost uninformative. However, \mathcal{G} is not injective for the quadratic multimodal problem, and the Lipschitz property does not hold for these discontinuous problems.

The reference posterior distribution is approximated by the MCMC method with a step size 1.0 and 5×10^6 samples (with a 10^6 sample burn-in period). The SMC method with 10^3 particles and 10^2 uniform steps is also applied for comparison. As for the UKI, 2 initial conditions are considered, which are $\theta_0 \sim \mathcal{N}(-1, 0.5^2)$ and $\theta_0 \sim \mathcal{N}(1, 0.5^2)$. We find that only the hyperbola discontinuous problem is sensitive to the initial covariance for the UKI.

The approximated posterior distributions are presented in [Figure 1](#). Here the UKI results are from the 20th iteration. For the quadratic multimodal problem, the posterior distribution is a multimodal distribution, therefore, the UKI can only capture one modal, that is close to the initial condition θ_0 . For the hyperbola discontinuous problem, the UKI initialized on the different branch from θ_{ref} diverges to $-\infty$; but the UKI initialized on the same branch from θ_{ref} converges to θ_{ref} with good covariance estimation. This reveals the gradient-based nature of UKI, in contrast to the sampling-based nature of MCMC or SMC. For other cases, the distributions obtained by the UKI match well with the distributions delivered by the MCMC. It is worth mentioning, the UKI requires only 20 iterations (60 forward solver evaluations), which is much cheaper than MCMC and SMC methods.

4.2. Nonlinear 2-Parameter Model Problem. The numerical experiment considered here is a counterexample against the ensemble Kalman filter, which is proposed in [\[55\]](#) and further used in [\[59, 56\]](#). Consider the one-dimensional elliptic boundary-value problem

$$(4.1) \quad -\frac{d}{dx} \left(\exp(\theta_{(1)}) \frac{d}{dx} p(x) \right) = 1, \quad x \in [0, 1]$$

with boundary conditions $p(0) = 0$ and $p(1) = \theta_{(2)}$. The solution for this problem is given by

$$p(x) = \theta_{(2)}x + \exp(-\theta_{(1)}) \left(-\frac{x^2}{2} + \frac{x}{2} \right).$$

The inverse problem is to solve for $\theta = (\theta_{(1)}, \theta_{(2)})^T$ with the observations $y = (p(x_1), p(x_2))^T$ at $x_1 = 0.25$ and $x_2 = 0.75$. The Bayesian inverse problem is formulated as

$$y = \mathcal{G}(\theta) + \eta \quad \text{and} \quad \mathcal{G}(\theta) = \begin{bmatrix} p(x_1, \theta) \\ p(x_2, \theta) \end{bmatrix},$$

here $\mathcal{G}(\theta)$ is the forward model operator. The observation is $y = (27.5, 79.7)^T$ with observation error $\eta \sim \mathcal{N}(0, 0.1^2 \mathbb{I})$. And the prior is $\mathcal{N}(0, 10^2 \mathbb{I})$, which is almost uninformative.

The reference posterior distribution is approximated by the MCMC method with a step size 1.0 and 5×10^6 samples (with a 10^6 sample burn-in period). For the UKI, the initial condition is $\theta_0 \sim \mathcal{N}(0, \text{diag}\{1, 10^2\})$. The posterior distributions obtained by the UKI at the 5th, 10th, and 15th iterations are depicted in [Figure 2](#). The mean converges efficiently to the true value θ_{ref} and the covariance obtained by the UKI matches well with that obtained by MCMC.

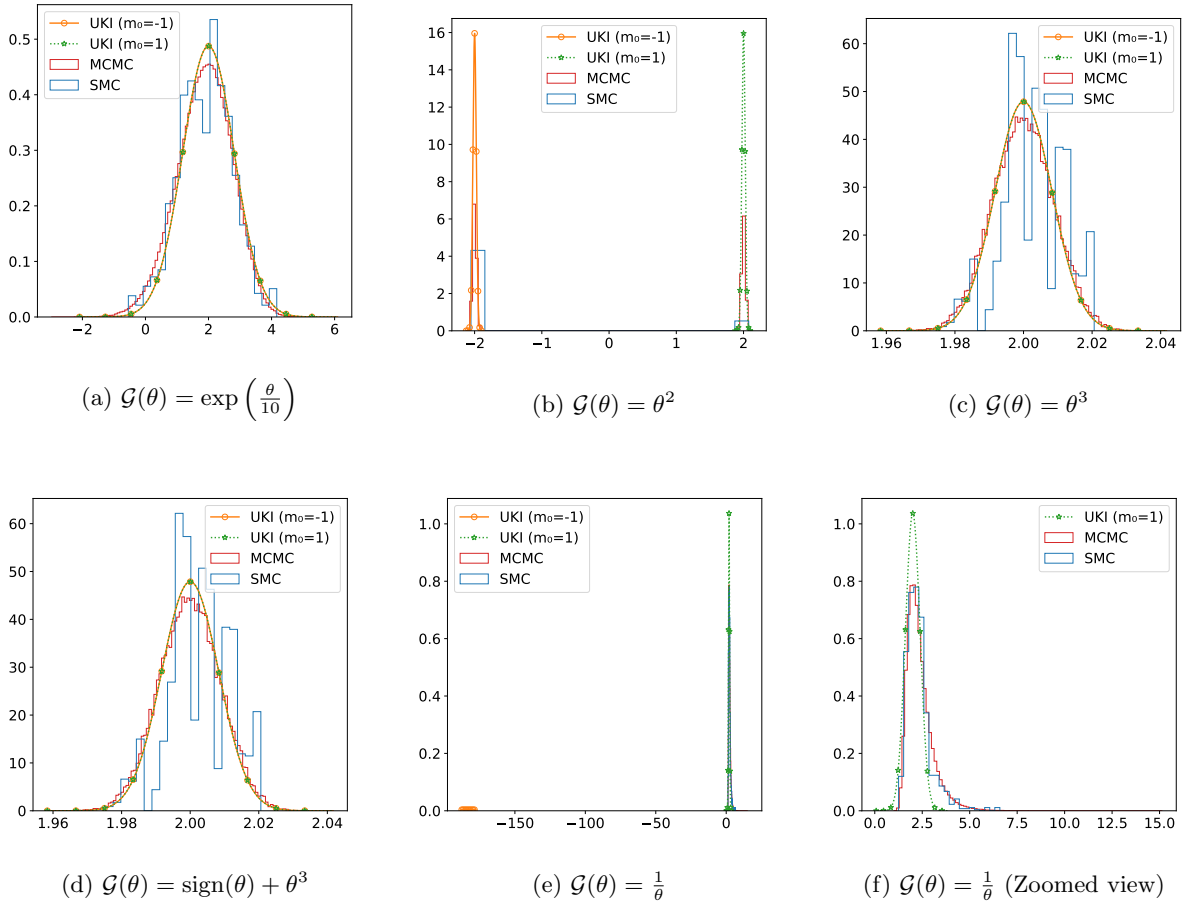


Fig. 1: Estimated posterior distributions by different approaches for different nonlinear 1-parameter model problems.

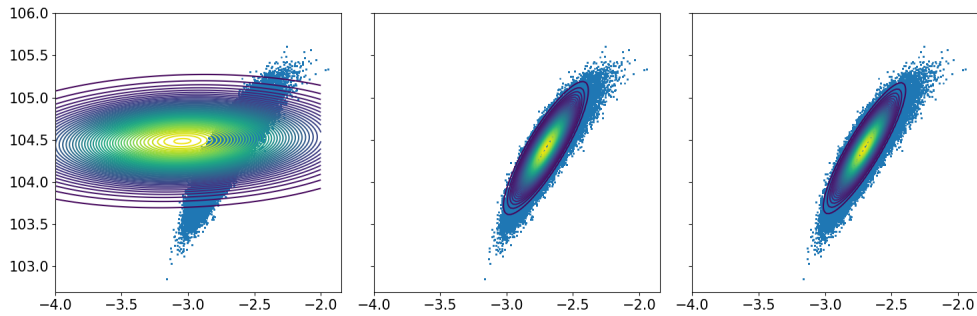


Fig. 2: Contour plot: posterior distributions obtained by UKI at 5th, 10th, and 15th iterations (from left to right); blue dots: reference posterior distribution obtained by MCMC for the 2-parameter model problem. x-axis is for $\theta_{(1)}$ and y-axis is for $\theta_{(2)}$.

4.3. Nonlinear High-Dimensional Model Problem. A similar one-dimensional elliptic boundary-value problem but with high-dimensional parameters is considered in this section. The equation describes

the pressure field $p(x)$ in a porous medium defined by a positive random permeability field $a(x, \theta)$:

$$(4.2) \quad -\frac{d}{dx} \left(a(x, \theta) \frac{d}{dx} p(x) \right) = f(x), \quad x \in [0, 1].$$

Here Dirichlet boundary conditions on the pressure are applied with $p(0) = 0$ and $p(1) = 0$, and f defines the source of the fluid:

$$f(x) = \begin{cases} 1000 & 0 \leq x \leq \frac{1}{2} \\ 2000 & \frac{1}{2} < x \leq 1 \end{cases}.$$

The random log-permeability field $\log a(x, \theta)$, depending on parameters $\theta \in \mathbb{R}^{N_\theta}$, is modeled as a log-Gaussian field with covariance operator

$$C = (-\Delta + \tau^2)^{-d},$$

where $-\Delta$ denotes the Laplacian on D subject to homogeneous Neumann boundary conditions on the space of spatial-mean zero functions, $\tau > 0$ denotes the inverse length scale of the random field and $d > 0$ determines its regularity ($\tau = 3$ and $d = 1$ in the present study²).

The log-Gaussian field is approximated by the following Karhunen-Loève (KL) expansion

$$(4.3) \quad \log a(x, \theta) = \sum_{l=1}^{+\infty} \theta_{(l)} \sqrt{\lambda_l} \psi_l(x),$$

and the eigenpairs are of the form

$$\psi_l(x) = \sqrt{2} \cos(\pi l x) \quad \text{and} \quad \lambda_l = (\pi^2 l^2 + \tau^2)^{-d},$$

and $\theta_{(l)} \sim \mathcal{N}(0, 1)$ i.i.d. The forward problem is solved by the finite difference method with 512 grid points.

For the inverse problem, we generate a truth random field $\log a(x, \theta_{ref})$ with $N_\theta = 32$ and $\theta_{ref} \sim \mathcal{N}(0, \mathbb{I}^{32})$, which consists of the first 32 KL modes (See Figure 3-left). The observation y_{ref} consists of pointwise measurements of the pressure value $p(x)$ at 63 equidistant points in the domain (See Figure 3-right), with the observation error $\eta \sim \mathcal{N}(0, 0.1^2 \mathbb{I})$. The prior is $\mathcal{N}(0, 10^2 \mathbb{I})$, where the covariance is large, and therefore the prior is almost uninformative.

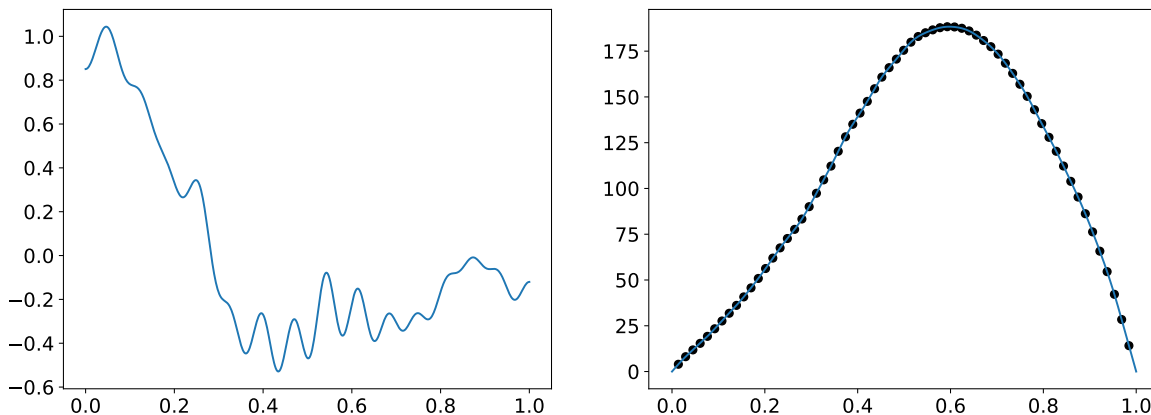


Fig. 3: The reference log-permeability field $\log a(x, \theta_{ref})$ (left) and the pressure field with 63 equidistant pointwise measurements (right) of the Darcy flow problem.

The reference posterior distribution is approximated by MCMC with 2×10^8 samples (with a 10^8 sample burn-in period). In order to accelerate the convergence of MCMC, we initialize the sampling with θ_{ref} and choose a step size 10^{-3} . For the UKI, the initial condition is $\theta_0 \sim \mathcal{N}(0, \mathbb{I})$.

² $d = 1$ ensures the eigenvalues do not decay too fast, and hence all parameters are effective.

The estimated KL expansion parameters $\{\theta_{(i)}\}$ for the log-permeability field and the associated $3\text{-}\sigma$ confidence intervals obtained by the UKI at the 20th iteration and MCMC are depicted in [Figure 4](#). Both UKI and MCMC converge to the true value θ_{ref} (the relative L_2 error $\frac{\|m_n - \theta_{ref}\|_2}{\|\theta_{ref}\|_2}$ obtained by UKI at the 20 iteration is about 10^{-2}), and the covariance estimations for each parameter match well with each other. The covariance for each pair $(\theta_{(i)}, \theta_{(j)})$ with $i \leq j$ obtained by UKI and MCMC are depicted in [Figure 5](#). These pairs are sorted in an ascent order by comparing the first element and then the second. The UKI and MCMC deliver very similar covariance estimations, which conforms to the theoretical results in [subsection 3.2](#).

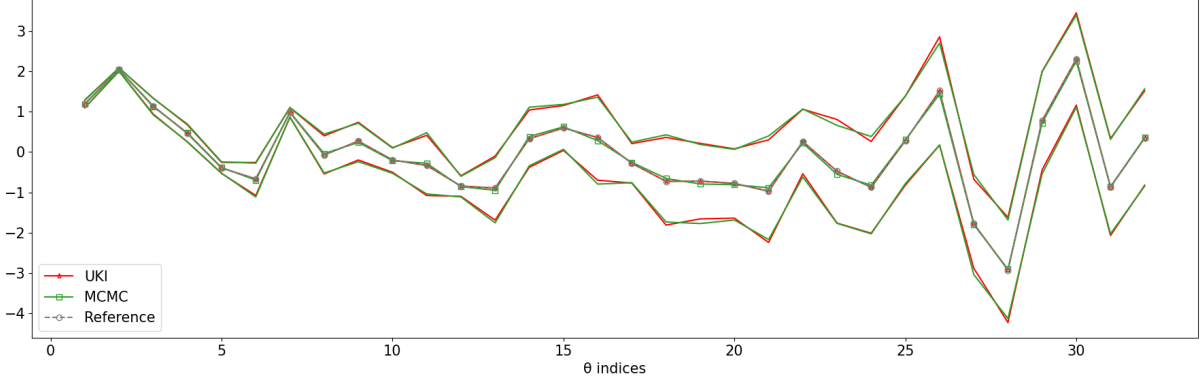


Fig. 4: The estimated KL expansion parameters $\theta_{(i)}$ and the associated $3\text{-}\sigma$ confidence intervals obtained by UKI and MCMC for the Darcy flow problem.

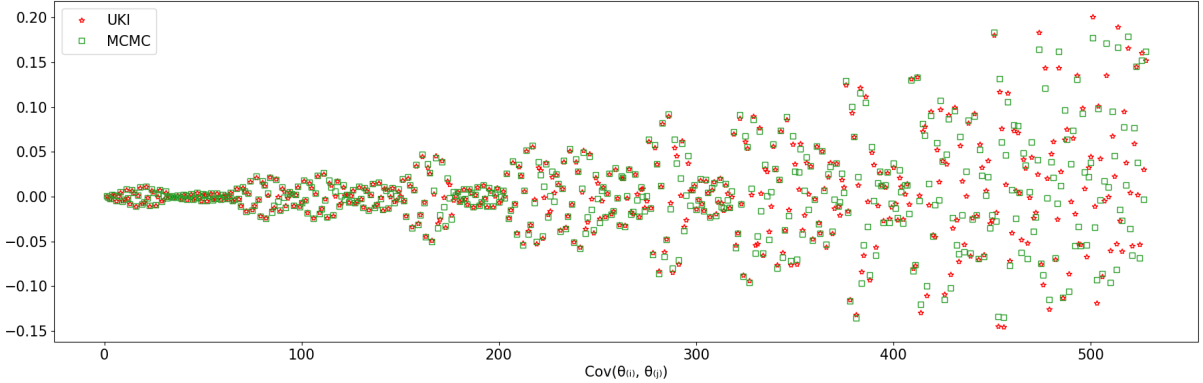


Fig. 5: The estimated covariance for each parameter pair $(\theta_{(i)}, \theta_{(j)})$ obtained by UKI and MCMC for the Darcy flow problem.

4.4. Navier-Stokes Problem. Finally, we consider the 2D Navier-Stokes equation on a periodic domain $D = [0, 2\pi] \times [0, 2\pi]$:

$$\begin{aligned} \frac{\partial v}{\partial t} + (v \cdot \nabla)v + \nabla p - \nu \Delta v &= 0, \\ \nabla \cdot v &= 0, \\ \frac{1}{4\pi^2} \int v &= v_b, \end{aligned}$$

here v and p denote the velocity vector and the pressure, $\nu = 0.01$ denotes the dynamic viscosity, and $v_b = (2\pi, 2\pi)$ denotes the non-zero mean background velocity. The forward problem is rewritten in the vorticity-stream ($\omega - \psi$) formulation:

$$\begin{aligned}\frac{\partial \omega}{\partial t} - (v \cdot \nabla)\omega - \nu \Delta \omega &= 0, \\ \omega &= -\nabla \psi \quad \frac{1}{4\pi^2} \int \psi = 0, \\ v &= \left(\frac{\partial \psi}{\partial x_2}, -\frac{\partial \psi}{\partial x_1} \right) + v_b,\end{aligned}$$

and solved by the pseudo-spectral method [60] on a 128×128 grid. To eliminating the aliasing error, the Orszag 2/3-Rule [61] is applied and, therefore there are 85^2 Fourier modes (padding with zeros). The time-integrator is the Crank–Nicolson method with $\Delta T = 2.5 \times 10^{-4}$.

The random initial vorticity field $\omega_0(x, \theta)$, depending on parameters $\theta \in \mathbb{R}^{N_\theta}$, is modeled as a Gaussian random field with covariance operator $\mathbf{C} = \Delta^{-2}$, which subjects to periodic boundary conditions on the space of spatial-mean zero functions. The KL expansion of the initial vorticity field is given by

$$(4.4) \quad \omega_0(x, \theta) = \sum_{l \in K} \theta_{(l)}^c \sqrt{\lambda_l} \psi_l^c + \theta_{(l)}^s \sqrt{\lambda_l} \psi_l^s,$$

where $K = \{(k_x, k_y) | k_x + k_y > 0 \text{ or } (k_x + k_y = 0 \text{ and } k_x > 0)\}$, and the eigenpairs are of the form

$$\psi_l^c(x) = \frac{\cos(l \cdot x)}{\sqrt{2\pi}} \quad \psi_l^s(x) = \frac{\sin(l \cdot x)}{\sqrt{2\pi}} \quad \lambda_l = \frac{1}{|l|^4},$$

and $\theta_{(l)}^c, \theta_{(l)}^s \sim \mathcal{N}(0, 2\pi^2)$ i.i.d. The KL expansion (4.4) can be rewritten as a sum over \mathbb{Z}^{0+} rather than a lattice:

$$(4.5) \quad \omega_0(x, \theta) = \sum_{k \in \mathbb{Z}^{0+}} \theta_{(k)} \sqrt{\lambda_k} \psi_k(x),$$

where the eigenvalues λ_k are in descending order.

For the inverse problem, we recover the initial condition, specifically the initial vorticity field of the Navier-Stokes equation, given pointwise observations y_{ref} of the vorticity field at 64 equidistant points ($N_y = 128$) at $T = 0.25$ and $T = 0.5$ (See Figure 6). And 5% Gaussian random noises are added to the observation, as follows,

$$y_{obs} = y_{ref} + 5\% y_{ref} \odot \mathcal{N}(0, \mathbb{I}),$$

here \odot denotes element-wise multiplication. The observation error is $\eta \sim \mathcal{N}(0, 0.1^2 \mathbb{I})$, which corresponds to the noise level. The initial vorticity field is generated with 100 Fourier modes of (4.4), and the first 50 modes are recovered ($N_\theta = 100$), and hence the model is misspecified and model error exists. The UKI is initialized with $\theta_0 \sim \mathcal{N}(0, \mathbb{I})$.

The convergence of the initial vorticity field $\omega_0(x, m_n)$, the optimization errors, and the Frobenius norm of the covariance are depicted in Figure 7. Thanks to the linear (or superlinear) convergence rate of the LMA [1], the UKI converges efficiently.

The truth random initial vorticity field $\omega_0(x, \theta_{ref})$ and the initial vorticity field recovered by UKI at the 20th iteration are depicted in Figure 8. The UKI captures well main features of the truth random initial field and even small features, despite the irreversibility of the diffusion process ($\nu = 0.01$). The estimated parameters $\{\theta_{(l)}^c\}, \{\theta_{(l)}^s\}$, and the associated 3- σ confidence intervals obtained by the UKI are depicted in Figure 9. Most of the reference values are in the confidence interval.

5. Conclusion. Unscented Kalman inversion is proposed as a derivative-free optimization method for inverse problems. In this paper, we further study the capability of UKI for Bayesian inference and uncertainty quantification. We focus on identifiable inverse problems, since a wide range of inverse problems belong to this category, especially with the availability of large and diverse data sets from experiments and direct

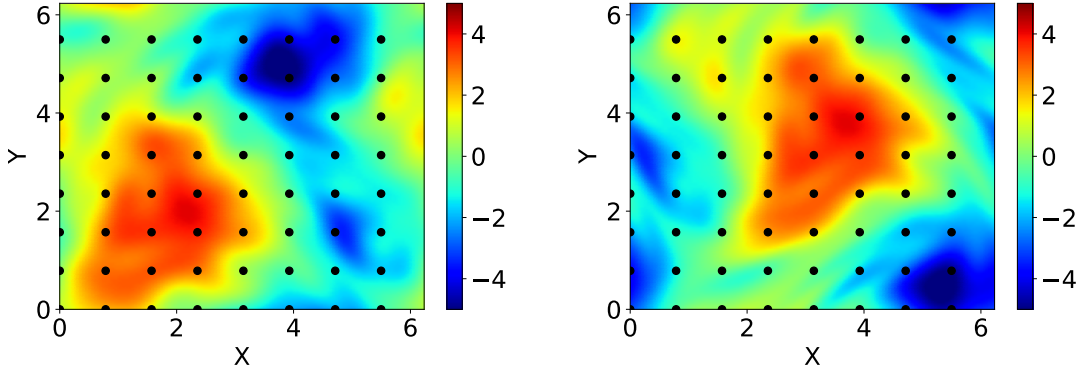


Fig. 6: The vorticity field of the Navier-Stokes problem and the 64 equidistant pointwise measurements (black dots) at two observation times ($T = 0.25$ and $T = 0.5$).

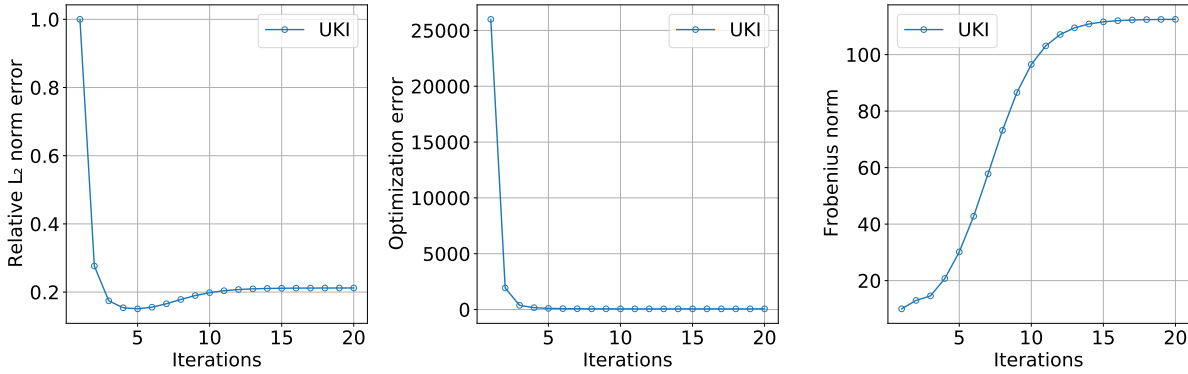


Fig. 7: Relative error $\frac{\|\omega_0(x, m_n) - \omega_{0,ref}\|_2}{\|\omega_{0,ref}\|_2}$ (left), the optimization error $\frac{1}{2} \|\Sigma_\nu^{-\frac{1}{2}}(y_{obs} - \hat{y}_n)\|^2$ (middle), and the Frobenius norm of covariance $\|C_n\|_F$ for the Navier-Stokes initial inverse problem.

simulations. Theoretical guarantees are presented, for linear inverse problems, the mean and covariance obtained by the UKI converge exponentially fast to the posterior mean and covariance; for nonlinear inverse problems, the error bounds of the mean and covariance are derived, in terms of the observation error. Numerical studies empirically confirm the theoretical results and demonstrate the effectiveness of UKI as an efficient Bayesian inference tool. For the Navier-Stokes problem, the model error exists. It is interesting to systematically quantify model-form error by using UKI in the future.

Acknowledgments. D.Z.H. is supported by the generosity of Eric and Wendy Schmidt by recommendation of the Schmidt Futures program. J.H. is supported by the Simons Foundation as a Junior Fellow at New York University.

Appendix A. Gaussian Approximation. For the Gaussian approximation in [subsection 2.1](#), assume the distribution of $\theta_n|Y_n$ is $\mu_n = \mathcal{N}(m_n, C_n)$, then the distribution of $\theta_{n+1}|Y_n$ is $\hat{\mu}_{n+1} = \mathcal{N}(\hat{m}_{n+1}, \hat{C}_{n+1})$. The joint density function of $\{\theta_{n+1}, y_{n+1}\}|Y_n$ is $p(\theta, y)$:

$$(A.1) \quad p(\theta_{n+1}, y_{n+1}|Y_n) = p(y_{n+1}|\theta_{n+1}, Y_n)p(\theta_{n+1}|Y_n) \propto e^{-\Phi(\theta_{n+1}, y_{n+1})} p_0(\theta_{n+1}),$$

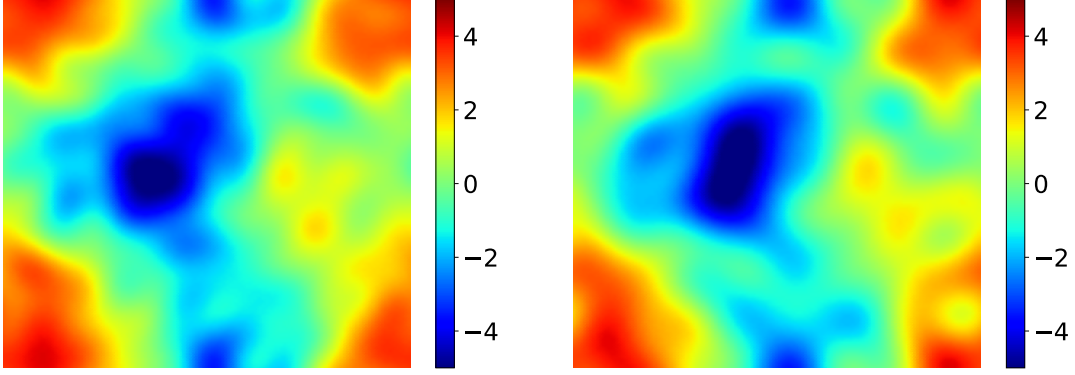


Fig. 8: Truth initial vorticity field $\omega_0(x, \theta_{ref})$ (left) and the Initial vorticity fields $\omega_0(x, m_n)$ recovered by the UKI (right) for the Navier-Stokes problem.

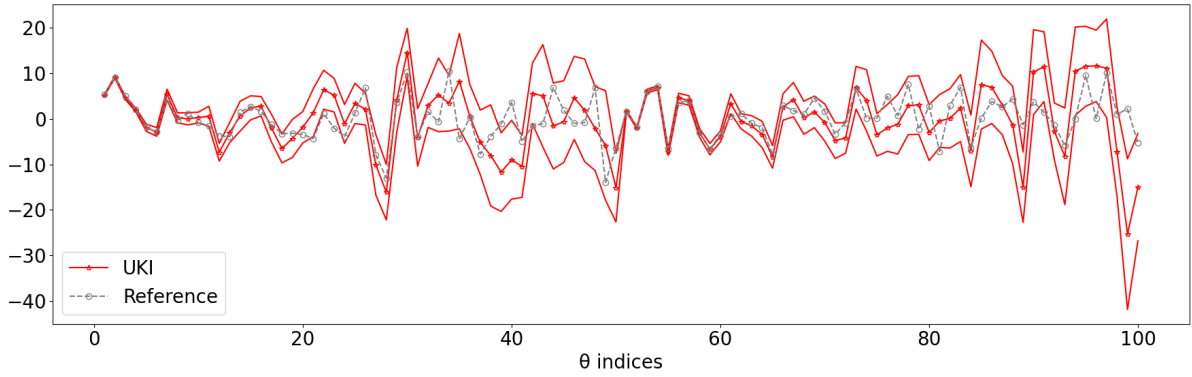


Fig. 9: The estimated Fourier expansion parameters $\{\theta_{(l)}^c\}, \{\theta_{(l)}^s\}$ and the associated 3- σ confidence intervals obtained by UKI for the Navier-Stokes problem.

where p_0 is the density function of $\theta_{n+1}|Y_n$. The Gaussian approximated joint density function is $p^G(\theta, y)$

$$(A.2) \quad p^G(\theta_{n+1}, y_{n+1}|Y_n) = \mathcal{N}\left(\begin{bmatrix} \hat{m}_{n+1} \\ \hat{y}_{n+1} \end{bmatrix}, \begin{bmatrix} \hat{C}_{n+1} & \hat{C}_{n+1}^{\theta p} \\ \hat{C}_{n+1}^{\theta p T} & \hat{C}_{n+1}^{pp} \end{bmatrix}\right),$$

It is worth mentioning $p(\theta, y)$ and $p^G(\theta, y)$ have the same mean and covariance by the definition of p^G . To obtain an upper bound for the Kullback–Leibler divergence between the true distribution $\theta_{n+1}|Y_{n+1}$ and $\mathcal{N}(m_{n+1}, C_{n+1})$, we need the following theorem:

THEOREM A.1. *Let denote the joint density function of $x = (\theta; y)$*

$$(A.3) \quad p(x) = \frac{1}{\hat{Z}} e^{-Q(x) - \epsilon H(x)} \quad \text{with} \quad Q(x) = \frac{1}{2}(x - \hat{m})^T \hat{C}^{-1}(x - \hat{m}),$$

here $Q(x)$ represents the quadrature term, $\epsilon H(x)$ represents other terms and \hat{Z} is the normalization constant. Let \hat{m}^G and \hat{C}^G denote the mean and covariance of $p(x)$, the approximated joint Gaussian density function is

$$p^G(x) = \frac{1}{\hat{Z}^G} e^{-Q^G(x)} \quad \text{with} \quad Q^G(x) = \frac{1}{2}(x - \hat{m}^G)^T \hat{C}^{G^{-1}}(x - \hat{m}^G).$$

We assume

1. $\exists c_0 > 0$ and $c_1 > 0$, such that $|H(x)| \leq c_0 x^T x + c_1$, and $\lambda_{\min}(\widehat{C}^{-1}) > 2\epsilon c_0$,³
2. $\exists c_2 > 0$, such that $\lambda_{\min}(\widehat{C}) > c_2$, $\lambda_{\min}(\widehat{C}^{G^{-1}}) > c_2$, and $\lambda_{\min}(\widehat{C}^G) > c_2$,
3. $\dim(x)$, c_i , and each entry of y , \widehat{m} , \widehat{C} , \widehat{C}^{-1} , \widehat{m}^G , \widehat{C}^G , $\widehat{C}^{G^{-1}}$ are $\mathcal{O}(1)$ constants, and ϵ is small enough.

We have an upper bound for the Kullback–Leibler divergence between the conditional distributions:

$$(A.4) \quad \mathcal{D}_{KL}\left(p^G(\theta|y) \parallel p(\theta|y)\right) = \mathcal{O}(\epsilon).$$

Proof. We first prove

$$(A.5) \quad \|\widehat{m}^G - \widehat{m}\|_\infty = \mathcal{O}(\epsilon) \quad \text{and} \quad \|\widehat{C}^G - \widehat{C}\|_\infty = \mathcal{O}(\epsilon).$$

We denote the Gaussian distribution $p_0(x)$ with mean \widehat{m} and covariance \widehat{C} , and its associated expectation $\widehat{\mathbb{E}}[\cdot]$ as following,

$$p_0(x) = \frac{1}{Z_0} e^{-Q(x)} \quad \widehat{\mathbb{E}}[f] = \int f(x) p_0(x) dx.$$

Since we consider only mean and covariance, we restrict f to be x and xx^T in the following discussion. The expectation with respect to the density function $p(x)$ in (A.3) can be written as

$$(A.6) \quad \int f(x) p(x) dx = \frac{\widehat{\mathbb{E}}[f e^{-\epsilon H(x)}]}{\widehat{\mathbb{E}}[e^{-\epsilon H(x)}]},$$

which leads to

$$(A.7) \quad \begin{aligned} \int f(x) p(x) - f(x) p_0(x) d\theta &= \frac{\widehat{\mathbb{E}}[f(x) e^{-\epsilon H(x)}]}{\widehat{\mathbb{E}}[e^{-\epsilon H(x)}]} - \widehat{\mathbb{E}}[f(x)] \\ &= \int_0^\epsilon \partial_t \frac{\widehat{\mathbb{E}}[f(x) e^{-tH(x)}]}{\widehat{\mathbb{E}}[e^{-tH(x)}]} dt \\ &= \int_0^\epsilon \frac{\widehat{\mathbb{E}}[-f(x) H(x) e^{-tH(x)}]}{\widehat{\mathbb{E}}[e^{-tH(x)}]} + \frac{\widehat{\mathbb{E}}[f(x) e^{-tH(x)}] \widehat{\mathbb{E}}[H(x) e^{-tH(x)}]}{\widehat{\mathbb{E}}[e^{-tH(x)}]^2} dt. \end{aligned}$$

Since $\lambda_{\min}(\widehat{C}^{-1}) > 2\epsilon c_0$, $p_0(x) e^{\epsilon c_0 x^T x}$ decays exponentially. For $t \in [0, \epsilon]$, we have

$$(A.8) \quad \begin{aligned} \left| \frac{1}{\widehat{\mathbb{E}}[e^{-tH(x)}]} \right| &\leq \frac{1}{\widehat{\mathbb{E}}[e^{-\epsilon c_0 x^T x - \epsilon c_1}]} = \mathcal{O}(1), \\ \left\| \widehat{\mathbb{E}}[f(x) e^{-tH(x)}] \right\|_\infty &\leq \widehat{\mathbb{E}}[(\|x\|_\infty + N_\theta x^T x) e^{\epsilon c_0 x^T x + \epsilon c_1}] = \mathcal{O}(1), \\ \left\| \widehat{\mathbb{E}}[H(x) e^{-tH(x)}] \right\|_\infty &\leq \widehat{\mathbb{E}}[(c_0 x^T x + c_1) e^{\epsilon c_0 x^T x + \epsilon c_1}] = \mathcal{O}(1), \\ \left\| \widehat{\mathbb{E}}[f(x) H(x) e^{tH(x)}] \right\|_\infty &\leq \widehat{\mathbb{E}}[(\|x\|_\infty + N_\theta x^T x) (c_0 x^T x + c_1) e^{\epsilon c_0 x^T x + \epsilon c_1}] = \mathcal{O}(1). \end{aligned}$$

Plugging (A.8) into (A.7) leads to

$$(A.9) \quad \left\| \int f(x) p(x) - f(x) p_0(x) dx \right\|_\infty = \mathcal{O}(\epsilon),$$

which finishes the proof of (A.5).

Next, we define conditional distributions

$$p(\theta|y) = \frac{p(x)}{\int p(x) dy} := \frac{1}{Z(y)} e^{-Q(\theta|y) - \epsilon H(\theta, y)} \quad \text{and} \quad p^G(\theta|y) = \frac{p^G(x)}{\int p^G(x) dy} := \frac{1}{Z^G(y)} e^{-Q^G(\theta|y)},$$

³ $\lambda_{\min}(A)$ denotes the smallest eigenvalue of matrix A .

where

$$Q(\theta|y) = \frac{1}{2}(\theta - m)^T C^{-1}(\theta - m) \quad \text{and} \quad Q^G(\theta|y) = \frac{1}{2}(\theta - m^G)^T C^{G^{-1}}(\theta - m^G).$$

The conditional normal distribution theorem leads to

$$(A.10) \quad \begin{aligned} m &= \hat{m}_1 + \hat{C}_{12} \hat{C}_{22}^{-1} (y - \hat{m}_2) & \text{and} & \quad C = \hat{C}_{11} - \hat{C}_{12} \hat{C}_{22}^{-1} \hat{C}_{21}, \\ m^G &= \hat{m}_1^G + \hat{C}_{12}^G \hat{C}_{22}^{G^{-1}} (y - \hat{m}_2^G) & \text{and} & \quad C^G = \hat{C}_{11}^G - \hat{C}_{12}^G \hat{C}_{22}^{G^{-1}} \hat{C}_{21}^G, \end{aligned}$$

here the subscripts 1 and 2 correspond to θ and y components, respectively.

We then prove

$$(A.11) \quad \|m^G - m\|_\infty = \mathcal{O}(\epsilon) \quad \text{and} \quad \|C^G - C\|_\infty = \mathcal{O}(\epsilon).$$

Since $\lambda_{\min}(\hat{C}) > 2c_2$, we have

$$(A.12) \quad \lambda_{\min}(\hat{C}_{22}) = \min_{y^T y=1} y^T \hat{C}_{22} y = \min_{y^T y=1, \theta=0} (\theta; y)^T \hat{C}(\theta; y) \geq \min_{x^T x=1} x^T \hat{C} x = \lambda_{\min}(\hat{C}) > c_2,$$

and

$$(A.13) \quad \lambda_{\min}(\hat{C}_{22}^G) = \min_{y^T y=1} y^T \hat{C}_{22}^G y = \min_{y^T y=1, \theta=0} (\theta; y)^T \hat{C}^G(\theta; y) \geq \min_{x^T x=1} x^T \hat{C}^G x = \lambda_{\min}(\hat{C}^G) > c_2.$$

Bringing (A.5), (A.12), and (A.13) into (A.10) leads to (A.11).

Moreover, since the Schur complement C in (A.10) satisfies

$$(A.14) \quad \lambda_{\max}(\hat{C}) = \lambda_{\max} \left(\begin{bmatrix} C & \\ & 0 \end{bmatrix} + \begin{bmatrix} \hat{C}_{12} \hat{C}_{22}^{-1/2} \\ \hat{C}_{22}^{1/2} \end{bmatrix} \begin{bmatrix} \hat{C}_{22}^{-1/2} \hat{C}_{21} & \hat{C}_{22}^{1/2} \end{bmatrix} \right) \geq \lambda_{\max}(C),$$

we have

$$(A.15) \quad \lambda_{\min}(C^{-1}) \geq \lambda_{\min}(\hat{C}^{-1}) > 2\epsilon c_0 \quad \lambda_{\min}(C^{G^{-1}}) \geq \lambda_{\min}(\hat{C}^{G^{-1}}) > c_2.$$

Finally, the Kullback–Leibler divergence can be written as

$$(A.16) \quad \int p^G(\theta|y) \log \left(\frac{p^G(\theta|y)}{p(\theta|y)} \right) d\theta = \int p^G(\theta|y) \left(Q(\theta|y) + \epsilon H(\theta, y) - Q^G(\theta|y) + \log Z - \log Z^G \right) d\theta.$$

The first part of (A.16) can be written as

$$(A.17) \quad \begin{aligned} & \int p^G(\theta|y) \left(Q(\theta|y) + \epsilon H(\theta, y) - Q^G(\theta|y) \right) d\theta \\ &= \int p^G(\theta|y) \epsilon H(\theta, y) d\theta + \int p^G(\theta|y) \left(Q(\theta|y) - Q^G(\theta|y) \right) d\theta \\ &= \int p^G(\theta|y) \epsilon H(\theta, y) d\theta + \frac{1}{2} \text{tr}(C^{-1} C^G) + \frac{1}{2} (m^G - m)^T C^{-1} (m^G - m) - \frac{1}{2} \text{tr}(C^{G^{-1}} C^G) \\ &= \int p^G(\theta|y) \epsilon H(\theta, y) d\theta + \frac{1}{2} \text{tr} \left(C^{-1} (C^G - C) \right) + \frac{1}{2} (m^G - m)^T C^{-1} (m^G - m) \\ &= \mathcal{O}(\epsilon). \end{aligned}$$

For the second part of (A.16), let denote $Z_0 = \int e^{-Q(\theta|y)} d\theta$ and the expectation $\mathbb{E}[\cdot]$ with respect to the Gaussian distribution

$$p_0(\theta|y) = \frac{1}{Z_0(y)} e^{-Q(\theta|y)}.$$

Combining (A.15) and (A.8) leads to

$$(A.18) \quad \begin{aligned} \log Z - \log Z_0 &= \log \mathbb{E}[e^{-\epsilon H(\theta, y)}] = \int_0^\epsilon \partial_t \log \mathbb{E}[e^{-tH(\theta, y)}] dt = \int_0^\epsilon \frac{\mathbb{E}[-H(\theta, y)e^{-tH(\theta, y)}]}{\mathbb{E}[e^{-tH(\theta, y)}]} dt = \mathcal{O}(\epsilon), \\ \log Z_0 - \log Z^G &= \frac{1}{2} \left(\log \det C^G - \log \det C \right) = \mathcal{O}(\epsilon). \end{aligned}$$

Bringing (A.18) into the second part of (A.16) leads to

$$(A.19) \quad \int p^G(\theta|y) \left(\log Z - \log Z^G \right) d\theta = (\log Z - \log Z_0) + (\log Z_0 - \log Z^G) = \mathcal{O}(\epsilon). \quad \square$$

Combining (A.17) and (A.19) leads to the upper bound of the Kullback–Leibler divergence.

Following Theorem A.1, we assume Φ can be decomposed into the quadratic part $Q^\Phi(\theta, y)$ and the high order part $\epsilon H(\theta, y)$, as following

$$\Phi(\theta, y) = Q^\Phi(\theta, y) + \epsilon H(\theta, y),$$

which is true when $\mathcal{G}(\theta)$ is close to a linear function. We further define

$$Q(\theta, y) = Q^\Phi(\theta, y) + \frac{1}{2}(\theta - \hat{m}_{n+1})^T \hat{C}_{n+1}^{-1}(\theta - \hat{m}_{n+1}).$$

When Q and H satisfy the conditions in Theorem A.1, the conditional distribution $\mathcal{N}(m_{n+1}, C_{n+1})$ well approximates the true distribution $\theta_{n+1}|Y_{n+1}$.

Remark A.2. When \mathcal{G} is linear, namely $\Phi(\theta, y)$ is quadratic and $\epsilon = 0$, $\mathcal{N}(m_{n+1}, C_{n+1})$ is the exact distribution of $\theta_{n+1}|Y_{n+1}$.

Appendix B. Proof of Theorem 3.1.

Proof. With the hyperparameters defined in (2.13), the update equation of $\{C_n\}$ in (3.1) can be rewritten as

$$(B.1) \quad C_{n+1}^{-1} = G^T \Sigma_\nu^{-1} G + (C_n + \Sigma_\omega)^{-1} = \frac{1}{2} G^T \Sigma_\eta^{-1} G + (2C_n)^{-1}.$$

We have a close formula for C_n^{-1} :

$$(B.2) \quad C_n^{-1} = \left[1 - \frac{1}{2^n} \right] G^T \Sigma_\eta^{-1} G + \frac{1}{2^n} C_0^{-1}.$$

This leads to the exponential convergence $\lim_{n \rightarrow \infty} C_n^{-1} = G^T \Sigma_\eta^{-1} G$.

The convergence proof of m_n basically follows [1]. Equations (B.1) and (B.2) lead to

$$(B.3) \quad \frac{1}{2} G^T \Sigma_\eta^{-1} G = G^T \Sigma_\nu^{-1} G \preceq C_{n+1}^{-1} \preceq G^T \Sigma_\nu^{-1} G + \Sigma_+ \quad \text{where} \quad \Sigma_+ = G^T \Sigma_\nu^{-1} G + C_0^{-1}.$$

The update equation of m_n in (3.1) can be rewritten as

$$(B.4) \quad m_{n+1} = m_n + C_{n+1} G^T \Sigma_\nu^{-1} (y - G m_n).$$

Consider the $\text{Range}(G^T) \otimes \text{Ker}(G)$ decomposition of $m_n = m_n^\parallel + m_n^\perp$ with projections P_{G^\parallel} and P_{G^\perp} , we have

$$(B.5a) \quad m_{n+1}^\parallel = m_n^\parallel + P_{G^\parallel} C_{n+1} G^T \Sigma_\nu^{-1} (y - G m_n^\parallel),$$

$$(B.5b) \quad m_{n+1}^\perp = m_n^\perp + P_{G^\perp} C_{n+1} G^T \Sigma_\nu^{-1} (y - G m_n^\parallel).$$

Constraining on $\text{Range}(G^T)$, we have the fact that $B := G^T \Sigma_\nu^{-1} G$ is symmetric and $B \succ 0$. From this, it follows that $\mathbb{I} - \widehat{C}_{n+1} B$ has the same spectrum as $\mathbb{I} - B^{\frac{1}{2}} C_{n+1} B^{\frac{1}{2}}$. Using the bounds on C_{n+1} appearing in (B.3), the spectral radius of the update matrix in (B.5a) satisfies

$$\begin{aligned}
\rho(P_{G\parallel} - P_{G\parallel} C_{n+1} G^T \Sigma_\nu^{-1} G) &\leq \rho(P_{G\parallel}) \rho\left(\mathbb{I} - \sqrt{G^T \Sigma_\nu^{-1} G} C_{n+1} \sqrt{G^T \Sigma_\nu^{-1} G}\right) \\
\text{(B.6)} \qquad \qquad \qquad &\leq 1 - \rho\left(\sqrt{G^T \Sigma_\nu^{-1} G} (G^T \Sigma_\nu^{-1} G + \Sigma_+)^{-1} \sqrt{G^T \Sigma_\nu^{-1} G}\right) \\
&= 1 - \epsilon_0,
\end{aligned}$$

where $\epsilon_0 \in (0, 1)$. Hence, we have $\{m_n^\parallel\}$ converges exponentially to m_∞^\parallel , which satisfies $G^T \Sigma_\nu^{-1} (y - G m_\infty^\parallel) = 0$. The update equation (B.5b) of m_n^\perp can be written as

$$\text{(B.7)} \qquad \qquad \qquad m_{n+1}^\perp = m_n^\perp + P_{G^\perp} C_{n+1} G^T \Sigma_\nu^{-1} G (m_\infty^\parallel - m_n^\parallel).$$

Since $\rho(P_{G^\perp} C_{n+1} G^T \Sigma_\nu^{-1} G) \leq \rho(P_{G^\perp}) \leq 1$ and $\lim_{n \rightarrow \infty} m_n^\parallel - m_\infty^\parallel = 0$ converges exponentially fast, we have the exponential convergence of $\{m_n^\perp\}$ to m_∞^\perp . Therefore, the converged vector $m_\infty = m_\infty^\parallel + m_\infty^\perp$ satisfies $G^T \Sigma_\nu^{-1} (y - G m_\infty) = 0$, which is a minimizer of Φ . \square

Appendix C. Proof of Theorem 3.5.

Proof. Since we consider only mean and covariance, we consider function $f(\theta) = \theta$ or $\theta\theta^T$. The expectation with respect to the posterior distribution $p(\theta|y)$ is

$$\begin{aligned}
\mathbb{E}[f(\theta)|y] &= \int \frac{1}{Z} e^{-\Phi(\theta, y)} f(\theta) d\theta \\
\text{(C.1)} \qquad \qquad \qquad &= \frac{1}{Z} \int e^{-\frac{1}{2}(y - \mathcal{G}(\theta))^T \Sigma_\eta^{-1} (y - \mathcal{G}(\theta))} f(\theta) d\theta \\
&= \frac{1}{Z} \int e^{-\frac{1}{2}(y - \theta')^T \Sigma_\eta^{-1} (y - \theta')} f(\mathcal{G}^{-1}(\theta')) \left| \det \frac{d\mathcal{G}^{-1}(\theta')}{d\theta} \right| d\theta' \text{ where } \theta' = \mathcal{G}(\theta).
\end{aligned}$$

The expectation with respect to the pull-back distribution is

$$\begin{aligned}
\mathbb{E}[f(\theta^\eta)] &= \frac{1}{Z_\eta} \int f(\mathcal{G}^{-1}(y - \eta)) e^{-\frac{1}{2}\eta^T \Sigma_\eta^{-1} \eta} d\eta \\
\text{(C.2)} \qquad \qquad \qquad &= \frac{1}{Z_\eta} \int f(\mathcal{G}^{-1}(\theta')) e^{-\frac{1}{2}(y - \theta')^T \Sigma_\eta^{-1} (y - \theta')} d\theta' \text{ where } \theta' = y - \eta.
\end{aligned}$$

here $Z_\eta = \sqrt{(2\pi)^{N_y} \det \Sigma_\eta}$.

Let denote $\mathbb{E}_\theta[\cdot]$ the expectation with respect to the Gaussian density function $\mathcal{N}(y, \Sigma_\eta)$:

$$\text{(C.3)} \qquad \qquad \qquad \mathbb{E}_\theta[f] = \frac{1}{Z_\eta} \int e^{-\frac{1}{2}(y - \theta)^T \Sigma_\eta^{-1} (y - \theta)} f(\theta) d\theta,$$

The difference between these two expectations (C.1) and (C.2) becomes

$$\begin{aligned}
\mathbb{E}[f(\theta)|y] - \mathbb{E}[f(\theta^\eta)] &= \frac{1}{Z_\eta} \int e^{-\frac{1}{2}(y - \theta')^T \Sigma_\eta^{-1} (y - \theta')} f(\mathcal{G}^{-1}(\theta')) \left(\frac{\left| \det \frac{d\mathcal{G}^{-1}(\theta')}{d\theta} \right|}{Z/Z_\eta} - 1 \right) d\theta' \\
\text{(C.4)} \qquad \qquad \qquad &= \mathbb{E}_{\theta'} \left[f(\mathcal{G}^{-1}(\theta')) \left(\frac{\left| \det \frac{d\mathcal{G}^{-1}(\theta')}{d\theta} \right|}{\mathbb{E}_\theta \left| \det \frac{d\mathcal{G}^{-1}(\theta)}{d\theta} \right|} - 1 \right) \right].
\end{aligned}$$

Here we use

$$\frac{Z}{Z_\eta} = \mathbb{E}_\theta \left| \det \frac{d\mathcal{G}^{-1}(\theta)}{d\theta} \right|.$$

Since we have the Lipschitz property, this leads to

$$\begin{aligned}
\left| \frac{\left| \det \frac{d\mathcal{G}^{-1}(\theta')}{d\theta} \right|}{\mathbb{E}_\theta \left[\left| \det \frac{d\mathcal{G}^{-1}(\theta)}{d\theta} \right| \right]} - 1 \right| &= \left| \frac{\mathbb{E}_\theta \left[\left| \det \frac{d\mathcal{G}^{-1}(\theta')}{d\theta} \right| - \left| \det \frac{d\mathcal{G}^{-1}(\theta)}{d\theta} \right| \right]}{\mathbb{E}_\theta \left[\left| \det \frac{d\mathcal{G}^{-1}(\theta)}{d\theta} \right| \right]} \right| \\
&\leq \frac{\mathbb{E}_\theta \left[\left| \left| \det \frac{d\mathcal{G}^{-1}(\theta')}{d\theta} \right| - \left| \det \frac{d\mathcal{G}^{-1}(y)}{d\theta} \right| \right| \right] + \mathbb{E}_\theta \left[\left| \left| \det \frac{d\mathcal{G}^{-1}(y)}{d\theta} \right| - \left| \det \frac{d\mathcal{G}^{-1}(\theta)}{d\theta} \right| \right| \right]}{\mathbb{E}_\theta \left[\left| \det \frac{d\mathcal{G}^{-1}(\theta)}{d\theta} \right| \right]} \\
\text{(C.5)} \quad &\leq \frac{\mathbb{E}_\theta \left[c_0 \|\theta' - y\|^{c_1} + c_0 \|\theta - y\|^{c_1} \right]}{\mathbb{E}_\theta \left[\left| \det \frac{d\mathcal{G}^{-1}(\theta)}{d\theta} \right| \right]} \\
&= \frac{c_0 \|\theta' - y\|^{c_1} + c_0 \mathbb{E}_\theta \left[\|\theta - y\|^{c_1} \right]}{\mathbb{E}_\theta \left[\left| \det \frac{d\mathcal{G}^{-1}(\theta)}{d\theta} \right| \right]}.
\end{aligned}$$

Bringing (C.5) into (C.4) leads to

$$\begin{aligned}
&\left\| \mathbb{E}_{\theta'} \left[f(\mathcal{G}^{-1}(\theta')) \left(\frac{\left| \det \frac{d\mathcal{G}^{-1}(\theta')}{d\theta} \right|}{\mathbb{E}_\theta \left| \det \frac{d\mathcal{G}^{-1}(\theta)}{d\theta} \right|} - 1 \right) \right] \right\|_\infty \\
&\leq \frac{c_0 \mathbb{E}_{\theta'} \left[\left\| f(\mathcal{G}^{-1}(\theta')) \right\|_\infty \|\theta' - y\|^{c_1} \right]}{\mathbb{E}_\theta \left[\left| \det \frac{d\mathcal{G}^{-1}(\theta)}{d\theta} \right| \right]} + c_0 \mathbb{E}_{\theta'} \left[\left\| f(\mathcal{G}^{-1}(\theta')) \right\|_\infty \right] \frac{\mathbb{E}_\theta \left[\|\theta - y\|^{c_1} \right]}{\mathbb{E}_\theta \left[\left| \det \frac{d\mathcal{G}^{-1}(\theta)}{d\theta} \right| \right]} \\
&\leq \frac{c_0 \left(\mathbb{E}_{\theta'} \left[\left\| f(\mathcal{G}^{-1}(\theta')) \right\|_\infty^2 \right] \mathbb{E}_{\theta'} \left[\|\theta' - y\|^{2c_1} \right] \right)^{1/2}}{\mathbb{E}_\theta \left[\left| \det \frac{d\mathcal{G}^{-1}(\theta)}{d\theta} \right| \right]} + c_0 \mathbb{E}_{\theta'} \left[\left\| f(\mathcal{G}^{-1}(\theta')) \right\|_\infty \right] \frac{\mathbb{E}_\theta \left[\|\theta - y\|^{c_1} \right]}{\mathbb{E}_\theta \left[\left| \det \frac{d\mathcal{G}^{-1}(\theta)}{d\theta} \right| \right]} \\
&\leq \frac{c_0 \left(\mathbb{E}_{\theta'} \left[\left\| f(\mathcal{G}^{-1}(\theta')) \right\|_\infty^2 \right] \right)^{1/2}}{c_3/Z_\eta} \left(\mathbb{E}_{\theta'} \left[\|\theta' - y\|^{2c_1} \right] \right)^{1/2} + c_0 \mathbb{E}_{\theta'} \left[\left\| f(\mathcal{G}^{-1}(\theta')) \right\|_\infty \right] \frac{\mathbb{E}_\theta \left[\|\theta - y\|^{c_1} \right]}{c_3/Z_\eta} \\
&\leq \frac{2c_0(c_2 + N_y)}{c_3} \mathcal{O} \left(\rho(\Sigma_\eta)^{c_1} \sqrt{\det \Sigma_\eta} \right).
\end{aligned}$$

This leads to the bounds (3.5). □

Appendix D. Proof of Theorem 3.6.

Proof. The update equations of the ExKI in (2.7) and (2.8) can be written as

$$\begin{aligned}
\text{(D.1)} \quad m_{n+1} &= m_n + \widehat{C}_{n+1} d\mathcal{G}(m_n)^T \left(d\mathcal{G}(m_n) \widehat{C}_{n+1} d\mathcal{G}(m_n)^T + \Sigma_\nu \right)^{-1} (y - \mathcal{G}(m_n)), \\
C_{n+1} &= \widehat{C}_{n+1} - \widehat{C}_{n+1} d\mathcal{G}(m_n)^T \left(d\mathcal{G}(m_n) \widehat{C}_{n+1} d\mathcal{G}(m_n)^T + \Sigma_\nu \right)^{-1} d\mathcal{G}(m_n) \widehat{C}_{n+1},
\end{aligned}$$

where $\widehat{C}_{n+1} = C_n + \Sigma_\omega = 2C_n$. By applying Sherman–Morrison–Woodbury formula, the ExKI update equations (D.1) can be rewritten as

$$\begin{aligned}
\text{(D.2)} \quad m_{n+1} &= m_n + C_{n+1} d\mathcal{G}(m_n)^T \Sigma_\nu^{-1} (y - \mathcal{G}(m_n)), \\
C_{n+1}^{-1} &= \frac{1}{2} C_n^{-1} + d\mathcal{G}(m_n)^T \Sigma_\nu^{-1} d\mathcal{G}(m_n).
\end{aligned}$$

The stationery mean and covariance m_* , C_* of (D.2) satisfy

$$\begin{aligned}
\text{(D.3)} \quad 0 &= C_* d\mathcal{G}(m_*)^T \Sigma_\nu^{-1} (y - \mathcal{G}(m_*)), \\
C_*^{-1} &= \frac{1}{2} C_*^{-1} + d\mathcal{G}(m_*)^T \Sigma_\nu^{-1} d\mathcal{G}(m_*).
\end{aligned}$$

Since C_* and $d\mathcal{G}(m_*)$ are non-singular, they are uniquely determined as following,

$$m_* = \mathcal{G}^{-1}(y) \quad \text{and} \quad C_*^{-1} = d\mathcal{G}(m_*)^T \Sigma_\eta^{-1} d\mathcal{G}(m_*).$$

When the extended Kalman filter is applied to estimate the mean and covariance of the pull-back random variable $\theta^\eta = \mathcal{G}^{-1}(y - \eta)$, we have

$$\begin{aligned} \mathbb{E}[\theta^\eta] &:= \mathcal{G}^{-1}(y - \mathbb{E}\eta) = \mathcal{G}^{-1}(y) = m_*, \\ \text{Cov}[\theta^\eta] &:= d\mathcal{G}^{-1}(y) \text{Cov}[\eta] d\mathcal{G}^{-T}(y) = d\mathcal{G}^{-1}(y) \Sigma_\eta d\mathcal{G}^{-T}(y) = C_*. \end{aligned} \quad \square$$

REFERENCES

- [1] Daniel Z Huang, Tapio Schneider, and Andrew M Stuart. Unscented kalman inversion. *arXiv preprint arXiv:2102.01580*, 2021.
- [2] Daniel Z Huang and Jiaoyang Huang. Improve unscented kalman inversion with low-rank approximation and reduced-order model. *arXiv preprint arXiv:2102.10677*, 2020.
- [3] Mrinal K Sen and Paul L Stoffa. *Global optimization methods in geophysical inversion*. Cambridge University Press, 2013.
- [4] Tapio Schneider, Shiwei Lan, Andrew Stuart, and Joao Teixeira. Earth system modeling 2.0: A blueprint for models that learn from observations and targeted high-resolution simulations. *Geophysical Research Letters*, 44(24):12–396, 2017.
- [5] Oliver RA Dunbar, Alfredo Garbuno-Inigo, Tapio Schneider, and Andrew M Stuart. Calibration and uncertainty quantification of convective parameters in an idealized gcm. *arXiv preprint arXiv:2012.13262*, 2020.
- [6] Daniel Z Huang, Kailai Xu, Charbel Farhat, and Eric Darve. Learning constitutive relations from indirect observations using deep neural networks. *Journal of Computational Physics*, page 109491, 2020.
- [7] Kailai Xu, Daniel Z Huang, and Eric Darve. Learning constitutive relations using symmetric positive definite neural networks. *Journal of Computational Physics*, 428:110072, 2021.
- [8] Philip Avery, Daniel Z Huang, Wanli He, Johanna Ehlers, Armen Derkevorkian, and Charbel Farhat. A computationally tractable framework for nonlinear dynamic multiscale modeling of membrane fabric. *arXiv preprint arXiv:2007.05877*, 2020.
- [9] Brian H Russell. *Introduction to seismic inversion methods*. SEG Books, 1988.
- [10] Carey Bunks, Fatimetou M Saleck, S Zaleski, and G Chavent. Multiscale seismic waveform inversion. *Geophysics*, 60(5):1457–1473, 1995.
- [11] Subhadip Mukherjee, Sören Dittmer, Zakhar Shumaylov, Sebastian Lunz, Ozan Öktem, and Carola-Bibiane Schönlieb. Learned convex regularizers for inverse problems. *arXiv preprint arXiv:2008.02839*, 2020.
- [12] Flávio Celso Trigo, Raul Gonzalez-Lima, and Marcelo Britto Passos Amato. Electrical impedance tomography using the extended kalman filter. *IEEE Transactions on Biomedical Engineering*, 51(1):72–81, 2004.
- [13] Heinz Werner Engl, Martin Hanke, and Andreas Neubauer. *Regularization of inverse problems*, volume 375. Springer Science & Business Media, 1996.
- [14] Jari Kaipio and Erkki Somersalo. *Statistical and computational inverse problems*, volume 160. Springer Science & Business Media, 2006.
- [15] Masoumeh Dashti and Andrew M Stuart. The bayesian approach to inverse problems. *arXiv preprint arXiv:1302.6989*, 2013.
- [16] Rudolph Emil Kalman. A new approach to linear filtering and prediction problems. *J. Basic Eng. Mar.*, 82(1):35–45, 1960.
- [17] Harold Wayne Sorenson. *Kalman filtering: theory and application*. IEEE, 1985.
- [18] Geir Evensen. Sequential data assimilation with a nonlinear quasi-geostrophic model using monte carlo methods to forecast error statistics. *Journal of Geophysical Research: Oceans*, 99(C5):10143–10162, 1994.
- [19] Simon J Julier, Jeffrey K Uhlmann, and Hugh F Durrant-Whyte. A new approach for filtering nonlinear systems. In *Proceedings of 1995 American Control Conference-ACC'95*, volume 3, pages 1628–1632. IEEE, 1995.
- [20] Ienkaran Arasaratnam and Simon Haykin. Cubature kalman filters. *IEEE Transactions on automatic control*, 54(6):1254–1269, 2009.
- [21] Sharad Singhal and Lance Wu. Training multilayer perceptrons with the extended kalman algorithm. In *Advances in neural information processing systems*, pages 133–140, 1989.
- [22] Gintaras V Puskorius and Lee A Feldkamp. Decoupled extended kalman filter training of feedforward layered networks. In *IJCNN-91-Seattle International Joint Conference on Neural Networks*, volume 1, pages 771–777. IEEE, 1991.
- [23] Eric A Wan and Rudolph Van Der Merwe. The unscented kalman filter for nonlinear estimation. In *Proceedings of the IEEE 2000 Adaptive Systems for Signal Processing, Communications, and Control Symposium (Cat. No. 00EX373)*, pages 153–158. Ieee, 2000.
- [24] Yan Chen and Dean S Oliver. Ensemble randomized maximum likelihood method as an iterative ensemble smoother. *Mathematical Geosciences*, 44(1):1–26, 2012.
- [25] Marco A Iglesias, Kody JH Law, and Andrew M Stuart. Ensemble kalman methods for inverse problems. *Inverse Problems*, 29(4):045001, 2013.
- [26] Alexandre A Emerick and Albert C Reynolds. Investigation of the sampling performance of ensemble-based methods with a simple reservoir model. *Computational Geosciences*, 17(2):325–350, 2013.
- [27] Zhengyu Huang, Philip Avery, Charbel Farhat, Jason Rabinovitch, Armen Derkevorkian, and Lee D Peterson. Simulation

- of parachute inflation dynamics using an eulerian computational framework for fluid-structure interfaces evolving in high-speed turbulent flows. In *2018 AIAA Aerospace Sciences Meeting*, page 1540, 2018.
- [28] Daniel Z Huang, P-O Persson, and Matthew J Zahr. High-order, linearly stable, partitioned solvers for general multiphysics problems based on implicit-explicit runge-kutta schemes. *Computer Methods in Applied Mechanics and Engineering*, 346:674–706, 2019.
- [29] Daniel Z Huang, Will Pazner, Per-Olof Persson, and Matthew J Zahr. High-order partitioned spectral deferred correction solvers for multiphysics problems. *Journal of Computational Physics*, page 109441, 2020.
- [30] Daniel Z Huang, Philip Avery, Charbel Farhat, Jason Rabinovitch, Armen Derkevorkian, and Lee D Peterson. Modeling, simulation and validation of supersonic parachute inflation dynamics during mars landing. In *AIAA Scitech 2020 Forum*, page 0313, 2020.
- [31] Alistair Adcroft, Whit Anderson, V Balaji, Chris Blanton, Mitchell Bushuk, Carolina O Dufour, John P Dunne, Stephen M Griffies, Robert Hallberg, Matthew J Harrison, et al. The gfdl global ocean and sea ice model om4. 0: Model description and simulation features. *Journal of Advances in Modeling Earth Systems*, 11(10):3167–3211, 2019.
- [32] Charles S Peskin. Numerical analysis of blood flow in the heart. *Journal of computational physics*, 25(3):220–252, 1977.
- [33] Marsha Berger and Michael Aftosmis. Progress towards a cartesian cut-cell method for viscous compressible flow. In *50th AIAA Aerospace Sciences Meeting Including the New Horizons Forum and Aerospace Exposition*, page 1301, 2012.
- [34] Daniel Z Huang, Dante De Santis, and Charbel Farhat. A family of position-and orientation-independent embedded boundary methods for viscous flow and fluid-structure interaction problems. *Journal of Computational Physics*, 365:74–104, 2018.
- [35] Daniel Z Huang, Philip Avery, and Charbel Farhat. An embedded boundary approach for resolving the contribution of cable subsystems to fully coupled fluid-structure interaction. *International Journal for Numerical Methods in Engineering*, 2020.
- [36] Marsha J Berger, Phillip Colella, et al. Local adaptive mesh refinement for shock hydrodynamics. *Journal of computational Physics*, 82(1):64–84, 1989.
- [37] Raunak Borker, Daniel Huang, Sebastian Grimberg, Charbel Farhat, Philip Avery, and Jason Rabinovitch. Mesh adaptation framework for embedded boundary methods for computational fluid dynamics and fluid-structure interaction. *International Journal for Numerical Methods in Fluids*, 90(8):389–424, 2019.
- [38] Mohammad Zafari, Albert Coburn Reynolds, et al. Assessing the uncertainty in reservoir description and performance predictions with the ensemble kalman filter. In *SPE Annual Technical Conference and Exhibition*. Society of Petroleum Engineers, 2005.
- [39] Jeffrey L Anderson. An ensemble adjustment kalman filter for data assimilation. *Monthly weather review*, 129(12):2884–2903, 2001.
- [40] Craig H Bishop, Brian J Etherton, and Sharanya J Majumdar. Adaptive sampling with the ensemble transform kalman filter. part i: Theoretical aspects. *Monthly weather review*, 129(3):420–436, 2001.
- [41] Adrian Smith. *Sequential Monte Carlo methods in practice*. Springer Science & Business Media, 2013.
- [42] Peter K Kitaniidis. Quasi-linear geostatistical theory for inversing. *Water resources research*, 31(10):2411–2419, 1995.
- [43] Dean S Oliver, Nanqun He, and Albert C Reynolds. Conditioning permeability fields to pressure data. In *ECMOR V-5th European conference on the mathematics of oil recovery*, pages cp–101. European Association of Geoscientists & Engineers, 1996.
- [44] Sebastian Reich. A nonparametric ensemble transform method for bayesian inference. *SIAM Journal on Scientific Computing*, 35(4):A2013–A2024, 2013.
- [45] Pierre Del Moral, Arnaud Doucet, and Ajay Jasra. Sequential monte carlo samplers. *Journal of the Royal Statistical Society: Series B (Statistical Methodology)*, 68(3):411–436, 2006.
- [46] Nikolas Kantas, Alexandros Beskos, and Ajay Jasra. Sequential monte carlo methods for high-dimensional inverse problems: A case study for the navier-stokes equations. *SIAM/ASA Journal on Uncertainty Quantification*, 2(1):464–489, 2014.
- [47] Alexandros Beskos, Ajay Jasra, Ege A Muzaffer, and Andrew M Stuart. Sequential monte carlo methods for bayesian elliptic inverse problems. *Statistics and Computing*, 25(4):727–737, 2015.
- [48] Geir Evensen. The ensemble kalman filter for combined state and parameter estimation. *IEEE Control Systems Magazine*, 29(3):83–104, 2009.
- [49] Yaqing Gu and Dean S Oliver. The ensemble kalman filter for continuous updating of reservoir simulation models. 2006.
- [50] Marco A Iglesias. A regularizing iterative ensemble kalman method for pde-constrained inverse problems. *Inverse Problems*, 32(2):025002, 2016.
- [51] Claudia Schillings and Andrew M Stuart. Analysis of the ensemble kalman filter for inverse problems. *SIAM Journal on Numerical Analysis*, 55(3):1264–1290, 2017.
- [52] Claudia Schillings and Andrew M Stuart. Convergence analysis of ensemble kalman inversion: the linear, noisy case. *Applicable Analysis*, 97(1):107–123, 2018.
- [53] Marco Iglesias and Yuchen Yang. Adaptive regularisation for ensemble kalman inversion with applications to non-destructive testing and imaging. *arXiv preprint arXiv:2006.14980*, 2020.
- [54] Neil K Chada, Yuming Chen, and Daniel Sanz-Alonso. Iterative ensemble kalman methods: A unified perspective with some new variants. *arXiv preprint arXiv:2010.13299*, 2020.
- [55] Oliver G Ernst, Björn Sprungk, and Hans-Jörg Starkloff. Analysis of the ensemble and polynomial chaos kalman filters in bayesian inverse problems. *SIAM/ASA Journal on Uncertainty Quantification*, 3(1):823–851, 2015.
- [56] Alfredo Garbuno-Inigo, Franca Hoffmann, Wuchen Li, and Andrew M Stuart. Interacting langevin diffusions: Gradient structure and ensemble kalman sampler. *SIAM Journal on Applied Dynamical Systems*, 19(1):412–441, 2020.
- [57] Sebastian Reich and Colin Cotter. *Probabilistic forecasting and Bayesian data assimilation*. Cambridge University Press, 2015.
- [58] Kody Law, Andrew Stuart, and Kostas Zygalakis. Data assimilation. *Cham, Switzerland: Springer*, 2015.

- [59] Michael Herty and Giuseppe Visconti. Kinetic methods for inverse problems. *arXiv preprint arXiv:1811.09387*, 2018.
- [60] Jan S Hesthaven, Sigal Gottlieb, and David Gottlieb. *Spectral methods for time-dependent problems*, volume 21. Cambridge University Press, 2007.
- [61] Steven A Orszag and GS Patterson Jr. Numerical simulation of three-dimensional homogeneous isotropic turbulence. *Physical Review Letters*, 28(2):76, 1972.